

Coupling techniques for nonlinear ensemble filtering

Alessio Spantini, Ricardo Baptista, and Youssef Marzouk

Massachusetts Institute of Technology

Cambridge, MA 02139 USA

e-mail: spantini@mit.edu, rsb@mit.edu, ymarz@mit.edu

Abstract: We consider filtering in high-dimensional non-Gaussian state-space models with intractable transition kernels, nonlinear and possibly chaotic dynamics, and sparse observations in space and time. We propose a novel filtering methodology that harnesses transportation of measures, convex optimization, and ideas from probabilistic graphical models to yield robust ensemble approximations of the filtering distribution in high dimensions. Our approach can be understood as the natural generalization of the ensemble Kalman filter (EnKF) to *nonlinear* updates, using stochastic or deterministic couplings. The use of nonlinear updates can reduce the intrinsic bias of the EnKF at a marginal increase in computational cost. We avoid any form of importance sampling and introduce non-Gaussian localization approaches for dimension scalability. Our framework achieves state-of-the-art tracking performance on challenging configurations of the Lorenz-96 model in the chaotic regime.

Keywords and phrases: nonlinear filtering, state-space models, couplings, transport maps, ensemble Kalman filter, graphical models, localization, approximate Bayesian computation.

Contents

1	Introduction	2
1.1	Related work	4
1.2	Organization of the paper	6
1.3	Remarks on notation	6
2	Background on nonlinear filtering	7
2.1	State-space models	7
2.2	Two-step ensemble filtering	7
3	The stochastic and deterministic map filters	9
3.1	Analysis step with couplings	9
3.2	Knothe–Rosenblatt rearrangement	10
3.3	Stochastic map filter	11
3.4	Estimation of the Knothe–Rosenblatt rearrangement from samples	13
3.5	Regularization in high dimensions: localization of nonlinear maps	15
3.6	Remarks on the stochastic map filter	18
3.7	Deterministic map filter	21
4	Numerical experiments	24
4.1	Common aspects of the problem configurations	24
4.2	Lorenz-63	28

4.3	Lorenz-96 with long inter-observation time	29
5	Discussion	32
	Acknowledgments	34
A	Parameterization and computation of monotone triangular maps	34
B	Deterministic map filter with conditionally independent and local observations	37
C	Continuous ranked probability score evaluations	39
D	Effect of time discretization	39
E	Numerical results for Lorenz-96 model with heavy-tailed observational noise	40
F	Numerical results for Lorenz-96 model with nonlinear observations	41
	References	43

1. Introduction

State-space models formalize the probabilistic description of a time dependent latent process—the state—observed indirectly at discrete times [25]. These models can approximate a wide variety of stochastic processes, ranging from the evolution of atmospheric variables in meteorology to the volatility of financial assets. This paper is concerned with the problem of (discrete-time) *filtering*, i.e., characterizing the sequence of conditional distributions of the latent field at observation times, given all available measurements up to that time. Filtering arises in virtually every discipline that seeks an online integration of models with data, e.g., imaging, pharmacology, atmospheric sciences, and oceanography. In geophysical applications, filtering and several closely related inference problems (e.g., smoothing, sequential parameter inference) fall under the broad label of *data assimilation*.

Despite its importance and ubiquity, filtering remains a challenging task, particularly when (i) the state is high dimensional; (ii) the state transition dynamic is nonlinear, expensive to simulate, and intractable, e.g., if it involves the integration of a chaotic partial differential equation; and (iii) observations of the state are sparse, both in space and time [49, 64]. These constraints reflect typical challenges faced in numerical weather prediction or geophysical data assimilation, and pose severe challenges for *consistent* sequential Monte Carlo (SMC) algorithms, which invariably face particle degeneracy or impoverishment [69, 23]. In such scenarios, state-of-the-art results¹ are typically obtained with the ensemble Kalman filter (EnKF), which is the workhorse of modern ensemble-based data assimilation [26]. The EnKF implements a two-step Monte Carlo approximation of the classical Kalman recursions. In the *forecast* step, a particle approximation of the filtering distribution is propagated through the transition dynamic to yield a “forecast” ensemble at the next observation time. In the *analysis* step, the forecast ensemble is updated via the action of a *linear* transformation to yield an empirical approximation of the new filtering marginal. The linear transformation is estimated under Gaussian assumptions. Hence, the EnKF cannot yield consistent estimators of the filtering distribution for non-Gaussian models [50]. In essence, the EnKF trades consistency of the estimators for lower variance, and thus robustness in high dimensions. Yet the intrinsic bias of the EnKF—due both to

¹At least in terms of time-averaged errors in point estimates of the state [42].

the linear transformation and the way it is estimated—implies that increasing the ensemble size beyond a certain threshold does *not* improve accuracy; increasing computational effort does not yield better inference. We wish to address these limitations.

In this work, we introduce *non-Gaussian generalizations of the EnKF* by considering nonlinear transformations derived from couplings. Couplings provide a link between distributions. That is, for a pair of distributions (π_1, π_2) , a coupling is defined by a pair of random variables $(\mathbf{X}_1, \mathbf{X}_2)$, which admit π_1 and π_2 as marginal distributions [76]. We consider couplings that are induced by a continuous transformation T such that $\mathbf{X}_2 = T(\mathbf{X}_1)$. The transformation can be either deterministic or stochastic. When T is deterministic, we call it a *transport map* and say that the coupling is deterministic (see [76, Definition 1.2]). The transformation allows one to sample π_2 by evaluating T at samples from π_1 .

We interpret the analysis step of the EnKF as a problem of coupling the forecast distribution $\pi_{\mathbf{X}}$ with the filtering distribution $\pi_{\mathbf{X}|\mathbf{Y}}$. That is, given samples $\mathbf{x}^1, \dots, \mathbf{x}^M$ from $\pi_{\mathbf{X}}$ and a likelihood function $\pi_{\mathbf{Y}|\mathbf{X}}$, we seek a transformation T that yields samples $T(\mathbf{x}^1), \dots, T(\mathbf{x}^M)$ from $\pi_{\mathbf{X}|\mathbf{Y}}$. Couplings are not unique. We are particularly interested in transformations that can be estimated efficiently without resorting to importance sampling—perhaps using only convex optimization—and that are easy to “localize” in high dimensions. We want to avoid the use of weights and thus issues of particle degeneracy. Moreover, the computation of the transformation should *not* become increasingly challenging as the variance of the observation noise decreases. The latter is a typical concern of filtering algorithms that rely on some attributes—e.g., moments—of the bootstrap particle filter approximation. *This paper proposes two new algorithms*, called the stochastic and deterministic map filters. The former represents a non-Gaussian generalization of the EnKF with “perturbed observations” [15], while the latter is a nonlinear extension of the square-root EnKF [73].

The *stochastic map filter* seeks a non-deterministic transformation from forecast to filtering distribution. This transformation is given by a transport map that pushes forward the joint distribution of state *and* data at a given observation time, $\pi_{\mathbf{X},\mathbf{Y}}$, to the filtering distribution. We target a specific transport map derived from the Knothe–Rosenblatt (KR) rearrangement that pushes forward $\pi_{\mathbf{X},\mathbf{Y}}$ to a “reference” distribution with independent components, e.g., a standard normal. The KR rearrangement is the unique monotone triangular transport map that defines a deterministic coupling between two distributions [11], and can be estimated within a finite-dimensional function space using only *convex* optimization and samples from $\pi_{\mathbf{X},\mathbf{Y}}$ [58]. These samples are easy to obtain given a forecast ensemble $(\mathbf{x}^i)_{i \leq M}$: it suffices to simulate the likelihood $\pi_{\mathbf{Y}|\mathbf{X}}$ at each particle \mathbf{x}^i . If we restrict the estimator of the rearrangement to be linear, then we recover the stochastic EnKF [26]. If we consider nonlinear parameterizations of the estimator, however, we obtain a whole new class of nonlinear filtering algorithms, which rely on fast and robust convex optimization.

In the *deterministic map filter*, we adopt a complementary strategy and seek a deterministic transformation from the forecast to the filtering distribution. We view the transformation as a composition of two functions. The first function is a KR rearrangement

that pushes forward the forecast $\pi_{\mathbf{X}}$ to a reference distribution. This rearrangement can be estimated via convex optimization given only forecast samples, and yields an implicit approximation of the forecast density, $\hat{\pi}_{\mathbf{X}}$. The second function is a KR rearrangement that pushes forward the reference to an approximation of the filtering distribution given by $\hat{\pi}_{\mathbf{X}|\mathbf{Y}} \propto \pi_{\mathbf{Y}|\mathbf{X}} \hat{\pi}_{\mathbf{X}}$, which can be evaluated in closed form up to a normalizing constant. The estimation of the latter rearrangement leads to a variational problem, first proposed by [56], that is in general non-convex. This is an important difference with respect to the stochastic map filter, which relies entirely on convex optimization, at the cost of estimating higher-dimensional rearrangements. Yet, in the special case of local observations that are conditionally independent, we show how to implement the deterministic map filter using *only* convex optimization (Appendix B). The resulting scheme has a flavor similar to the multivariate rank histogram filter [53]. For a linear parameterization of the estimators *and* Gaussian likelihoods, the deterministic map filter reduces to a (deterministic) square-root EnKF [73]; otherwise, it is far more general.

In principle, both the stochastic and deterministic map filters can approximate a nonlinear update of arbitrary complexity: it suffices to enrich the function space for the estimator of the KR rearrangements. In practice, however, there is a tradeoff. Depending on the number of forecast particles M , overly complex parameterizations can lead to estimators with low bias but unacceptable variance, and vice-versa. Skillful filtering requires a careful balance between bias and variance. A key ingredient of the functional framework proposed in this paper is the ability to depart *gradually* from the linear ansatz. For example, in our numerical experiments we consider maps whose components are additively separable, as sums of univariate nonlinear functions. These parameterizations represent a natural extension of linear functions in terms of complexity, and lead to filtering algorithms that can outperform the EnKF at a marginal increase in computational cost and ensemble requirements (Section 4). Of course, more general parameterizations are also possible. In essence, we provide a natural tradeoff between computational cost and statistical accuracy—a tradeoff which is very limited in the EnKF, due to the restrictive linear ansatz.

In high-dimensional problems with limited ensemble sizes, we must further regularize the estimation of the rearrangements. In this paper, we introduce a notion of “localization” for nonlinear updates, by dropping some variable dependence from each component of the transport map. We show how *sparsity* of the KR rearrangement—a nonlinear function—is linked to properties of the filtering distribution, such as decay of correlation and (approximate) conditional independence [71]. Intuitively, these sparse transformations approximate the projection of the filtering distribution onto a manifold of non-Gaussian Markov random fields.

1.1. Related work

The idea of transporting measures via couplings has a long history [54, 76], and has found applications in fluid dynamics, economics, statistics, machine learning [24, 37, 56, 29], and many other fields. One of the first filtering algorithms to rely on the explicit construction

of (optimal) couplings is the ensemble transform particle filter [63, 1], which uses an importance sampling approximation of the filtering distribution—the same given by the bootstrap particle filter [30]—to obtain a consistent particle approximation of Monge’s optimal map [76] (cf. Section 3.1). Earlier work on particle flows investigated the use of transport maps induced by flows of ODEs [20]. Related ideas include the feedback particle filter [80] and the “Gibbs flow” [32]. In particular, [32] defines an approximation of the KR rearrangement between an input and a target measure via the solution of an ODE whose drift term depends only on the full conditionals of the target distribution. This approximation can be used as a proposal density for sequential Monte Carlo (SMC) methods. Also, the implicit sampling algorithm of [16, 55] defines a proposal density using an approximate transport map, which can be evaluated by solving a one-dimensional optimization problem: in this case, optimization is used to define the action of a single map, not to search for the best rearrangement within a class of candidate maps (see [52, Sec. 6] for more details). Among the flow methods, the variational mapping particle filter implements a particle flow given by a particular form of functional gradient descent on a reproducing kernel Hilbert space [61, 46]. We clarify its connection with the deterministic map filter in Section 3.7.

In our filters, we use a variational approximation of the KR rearrangement to Gaussianize a collection of particles. The idea of Gaussianizing multivariate data is well rooted in statistics [12], and is known as Gaussian anamorphosis (GA) in the geostatistics literature [77]. Usually, these approaches Gaussianize marginals of the data by estimating one-dimensional cumulative distribution functions. A typical application of GA within the context of non-Gaussian extensions of the EnKF is described in [2]: the idea is to (1) estimate a nonlinear transformation that Gaussianizes joint samples from the distribution of state *and* data at a given observation time, (2) derive an equivalent nonlinear observation operator in the transformed space, (3) apply EnKF formulas for nonlinear observation operators in the transformed space, and (4) map the analysis ensemble back to the original space. As explained in [2], this approach cannot recover the exact filtering distribution for non-Gaussian models, even if we had the *exact* nonlinear transformation. The problem is that we insist on using EnKF formulas in the transformed space. In the stochastic map filter introduced in this paper, on the other hand, we show how to bypass this issue by designing a nonlinear update that depends only on the nonlinear transformation that Gaussianizes the data. If we had the exact transformation, then the stochastic map filter would be exact.

Yet another measure transport approach to filtering is that of [71], which uses the idea of decomposable couplings to yield a recursive approximation of the full Bayesian solution to the sequential inference problem, using purely variational techniques (i.e., no sampling). See also [33] for a multilevel generalization of this variational method. Outside the coupling literature, an early attempt to devise non-Gaussian generalizations of the EnKF is the Gaussian mixture filter of [7]. Here, the idea is to learn the forecast density via a regularized mixture of Gaussians. Additional efforts at generalizing the EnKF to nonlinear updates include the hierarchical methods of [38], which complement the EnKF with a consistent Bayesian method, e.g., a particle filter, in a low-dimensional subspace of the variables of interest. The stochastic and deterministic map filters introduced in this paper could also be

adapted to this construction, after identifying a suitable decomposition of the variables. [21] analyzes stability properties of a class of (nonlinear) EnKFs that converge to the extended Kalman–Bucy filter as the number of particles goes to infinity. Finally, we note that complementary approaches to non-Gaussian high dimensional filtering include hybrid filters [27] and local weights particle filters [59]. These algorithms provide an alternative route to the regularization of SMC methods, which are usually consistent but plagued by large estimation variance in high dimensions. See [75] for a recent review.

1.2. Organization of the paper

The rest of the paper is organized as follows. In Section 2.1, we review the notion of state-space models. In Section 2.2, we describe the EnKF and discuss possible non-Gaussian generalizations. In Section 3.1, we interpret the analysis step of the EnKF as a problem of coupling the forecast distribution with the filtering distribution, and analyze the difference between stochastic and deterministic couplings. In Section 3.2, we recall properties of the KR rearrangement—a key coupling for our analysis. In Section 3.3, we introduce the stochastic map filter. In Section 3.4, we address estimation of the KR rearrangement via convex optimization, while in Section 3.5 we introduce regularization ideas for high dimensions. Specific parameterizations of the KR rearrangement are discussed in Appendix A. In Section 3.6, we collect a few remarks on the stochastic map filter, including the connection with the stochastic EnKF and additional localization ideas. In Section 3.7, we introduce the deterministic map filter. We report on our numerical experiments with chaotic dynamical systems in Section 4, evaluating both state estimation error and fidelity to the underlying Bayesian solution, among other performance metrics. Section 5 discusses open issues and outline directions for future work. Code and numerical examples are available online.²

1.3. Remarks on notation

For a pair of functions f and g , we denote their composition by $f \circ g$. We denote by $\partial_k f$ the partial derivative of f with respect to its k th input variable. We use boldface capital letters, e.g., \mathbf{X} , to denote random variables on \mathbb{R}^n , while we write scalar-valued random variables as X . For a density π , $\mathbf{X} \sim \pi$ means that \mathbf{X} is distributed according to π . For all $n > 0$, we let $\mathbb{N}_n = \{1, \dots, n\}$ denote the set of the first n integers. If $\mathbf{X} = (X_1, \dots, X_p)$ is a collection of random variables and $\mathcal{A} \subset \mathbb{N}_p$, then $\mathbf{X}_{\mathcal{A}} = (X_i, i \in \mathcal{A})$ denotes a subcollection of \mathbf{X} . In the same way, for $j < k$, $\mathbf{X}_{j:k} = (X_j, X_{j+1}, \dots, X_k)$. The same index notation applies to dummy variables $\mathbf{x} \in \mathbb{R}^n$. If $\mathbf{X} = (X_1, \dots, X_p)$ has joint density π and $\mathcal{A} \subset \mathbb{N}_p$, we denote by $\pi_{\mathbf{X}_{\mathcal{A}}}$ the marginal of π along $\mathbf{X}_{\mathcal{A}}$. If π is the density of $\mathbf{Z} = (\mathbf{X}, \mathbf{Y})$, we denote by $\pi_{\mathbf{X}|\mathbf{Y}}$ the density of \mathbf{X} given \mathbf{Y} . We denote independence of a pair of random variables \mathbf{X}, \mathbf{Y} by $\mathbf{X} \perp\!\!\!\perp \mathbf{Y}$. In the same way, $\mathbf{X} \perp\!\!\!\perp \mathbf{Y}|\mathbf{R}$ means that \mathbf{X} and \mathbf{Y} are independent given a third random variable \mathbf{R} .

²<https://github.com/map-filters>

2. Background on nonlinear filtering

2.1. State-space models

We consider a nonlinear, non-Gaussian state-space model given by a pair of discrete-time stochastic processes, $(\mathbf{Z}_k, \mathbf{Y}_k)$ for $k \geq 1$, where \mathbf{Z}_k denotes the unobserved state of a Markov chain taking values in \mathbb{R}^n , while (\mathbf{Y}_k) refers to an observed process in \mathbb{R}^d that is conditionally independent given the states at all times. In filtering, we want to leverage realizations $(\mathbf{y}_k)_{k \geq 1}$ of the observed process to infer the distribution of the latent state conditioned on all available measurements, i.e., we want to estimate the sequence of conditionals

$$\pi_{\mathbf{Z}_k | \mathbf{y}_{1:k}}(\mathbf{z}) := \pi_{\mathbf{Z}_k | \mathbf{Y}_1, \dots, \mathbf{Y}_k}(\mathbf{z} | \mathbf{y}_1, \dots, \mathbf{y}_k), \quad (2.1)$$

recursively in time, for all $k \geq 1$.

The joint law of the process $(\mathbf{Z}_k, \mathbf{Y}_k)$ is fully specified by the sequence of transition kernels $(\pi_{\mathbf{Z}_{k+1} | \mathbf{Z}_k})$ and likelihood functions $(\pi_{\mathbf{Y}_k | \mathbf{Z}_k})$, together with a distribution on the initial conditions of the latent process. We can think of \mathbf{Y}_k as an indirect and noisy observation of \mathbf{Z}_k , e.g.,

$$\mathbf{Y}_k = h(\mathbf{Z}_k, \boldsymbol{\mathcal{E}}_k) \quad (2.2)$$

for some mapping h and “noise” random variable $\boldsymbol{\mathcal{E}}_k$. In particular, the likelihood function $\pi_{\mathbf{Y}_k | \mathbf{Z}_k}$ need *not* be Gaussian. Moreover, in many cases $(\mathbf{Z}_k)_{k \geq 1}$ represents a subcollection of random variables from a larger state process—e.g., $(\mathbf{Z}_{j/\Delta})_{j \in \mathbb{N}}$ for some integer Δ —that is only observed at certain times $k = j/\Delta \in \mathbb{N}$ (see Figure 1). We thus consider settings with *sparse* measurements, both in space and time.

Example 1 (State-space model). *A possible dynamic for the state is given by $\mathbf{Z}_0 \sim \mathcal{N}(\mathbf{0}, \mathbf{I})$, and by a set of stochastic difference equations of the form*

$$\mathbf{Z}_{j+\frac{1}{\Delta}} = f(\mathbf{Z}_j) + \boldsymbol{\mathcal{W}}_j, \quad \forall j = 0, 1/\Delta, 2/\Delta, \dots, \quad (2.3)$$

for some deterministic forward model $f : \mathbb{R}^n \rightarrow \mathbb{R}^n$ and i.i.d. $(\boldsymbol{\mathcal{W}}_j) \sim \mathcal{N}(\mathbf{0}, \mathbf{I}/\Delta)$. Sampling from $\pi_{\mathbf{Z}_{k+1} | \mathbf{Z}_k}(\cdot | \mathbf{z})$ requires iterating over (2.3) for Δ times with initial conditions $\mathbf{Z}_0 = \mathbf{z}$. We can then consider that the state is observed through (\mathbf{Y}_k) only at integer times.

We assume that we can *sample* the transition kernel $\pi_{\mathbf{Z}_{k+1} | \mathbf{Z}_k}$, but not evaluate its density, which might not even exist when dealing with deterministic dynamics, e.g., $\boldsymbol{\mathcal{W}}_j = 0$ in (2.3).

2.2. Two-step ensemble filtering

We work with a general class of ensemble filtering algorithms, wherein the filtering distribution is approximated by a collection of particles that are updated recursively over time via a two-step process consisting of a *forecast* and an *analysis* step (Figure 2). The recursion takes a particle approximation $\mathbf{z}^1, \dots, \mathbf{z}^M$ of the filtering distribution $\pi_{\mathbf{Z}_k | \mathbf{y}_{1:k}}$ at time k , and

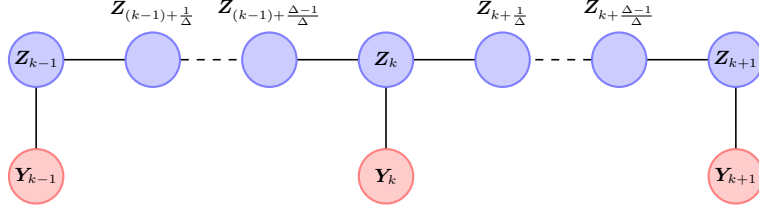


Fig 1: Markov structure for a state-space model consisting of a latent field $(\mathbf{Z}_{\frac{j}{\Delta}})_{j \in \mathbb{N}}$ which is observed every Δ time steps via a second stochastic process $(\mathbf{Y}_k)_{k \in \mathbb{N}}$.

turns it into a particle approximation of the filtering distribution at the next observation time, $\pi_{\mathbf{Z}_{k+1}|\mathbf{y}_{1:k+1}}$, by considering the following identity,

$$\pi_{\mathbf{Z}_{k+1}|\mathbf{Y}_{1:k+1}} \propto \pi_{\mathbf{Y}_{k+1}|\mathbf{Z}_{k+1}} \int \pi_{\mathbf{Z}_{k+1}|\mathbf{Z}_k} \pi_{\mathbf{Z}_k|\mathbf{Y}_{1:k}} d\mathbf{z}_k, \quad (2.4)$$

which links filtering marginals at consecutive observation times. In the forecast step, each particle \mathbf{z}^j is updated independently with a sample from $\pi_{\mathbf{Z}_{k+1}|\mathbf{Z}_k}(\cdot|\mathbf{z}^j)$, obtained by simulating the state dynamic until the next observation time. The resulting ensemble $\mathbf{z}_f^1, \dots, \mathbf{z}_f^M$ yields a particle approximation of the forecast (or predictive) distribution $\pi_{\mathbf{Z}_{k+1}|\mathbf{y}_{1:k}}$ —i.e., the distribution of the state at time $k+1$ conditioned on all observations available up to time k . The forecast step might involve the evaluation of an expensive forward model, like a partial differential equation, and represents the computational bottleneck for high dimensional and complex models, like those employed in weather forecasting. Yet, the forecast step is of little statistical concern, since we can usually sample *exactly* from $\pi_{\mathbf{Z}_{k+1}|\mathbf{Z}_k}$ up to the discretization of the forward model.³ The analysis step, however, is more challenging, since it involves the approximation of an inference task. We can think of the forecast distribution $\pi_{\mathbf{Z}_{k+1}|\mathbf{y}_{1:k}}$ as the prior of a Bayesian inverse problem, where the likelihood function and posterior distribution are given by $\pi_{\mathbf{y}_{k+1}|\mathbf{Z}_{k+1}}$ and $\pi_{\mathbf{Z}_{k+1}|\mathbf{y}_{1:k+1}}$, respectively. In the analysis step, we seek a particle approximation of the posterior $\pi_{\mathbf{Z}_{k+1}|\mathbf{y}_{1:k+1}}$ in a setting where the prior density $\pi_{\mathbf{Z}_{k+1}|\mathbf{y}_{1:k}}$ is not known explicitly, and where we only have finitely many samples $\mathbf{z}_f^1, \dots, \mathbf{z}_f^M$ from the prior.

The analysis step is thus a problem of approximate Bayesian inference, and can be implemented in various ways. For instance, the EnKF yields a particle approximation of the filtering distribution by pushing forward the forecast ensemble through a *linear* transformation estimated under Gaussian assumptions. In this paper, we leverage ideas from measure transport to generalize the EnKF by estimating *nonlinear* transformations in function space. Our goal is to reduce the estimation bias in the EnKF, while retaining applicability and robustness of the methodology in high dimensions.

³In this paper, for simplicity, we take the discretized model to be an exact representation of the forward dynamics.

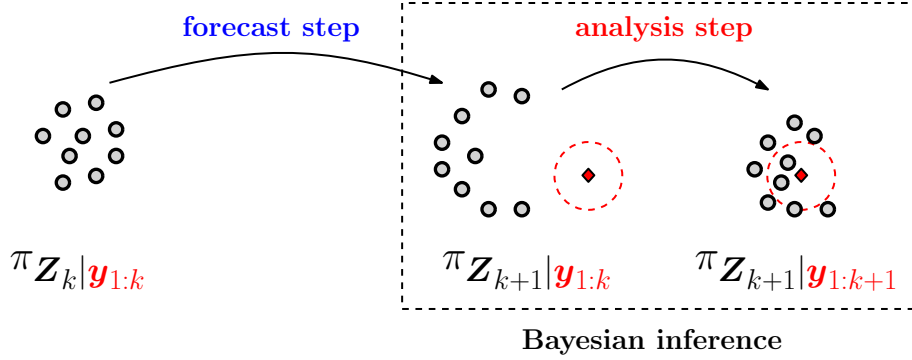


Fig 2: A typical ensemble filtering algorithm first propagates a particle approximation of the filtering distribution at time k until the next observation time $k + 1$ using the transition dynamic (*forecast step*). Then, it updates the ensemble via a transformation that incorporates information from the most recent observation \mathbf{y}_{k+1} (*analysis step*). The analysis step can be regarded as a problem of “static” Bayesian inference

3. The stochastic and deterministic map filters

In this section we introduce two novel methodologies for addressing the analysis step in nonlinear filtering problems. We start by framing the analysis step as a problem of coupling the forecast and the analysis distributions (in Section 3.1) and propose two solutions based on either stochastic (Section 3.3) or deterministic (Section 3.7) couplings.

3.1. Analysis step with couplings

The analysis step of the ensemble algorithms described in Section 2.2 can be formulated as an abstract Bayesian inference problem, defined by a pair of random variables (\mathbf{X}, \mathbf{Y}) on $\mathbb{R}^n \times \mathbb{R}^d$, which denote, respectively, the unobserved state variable and the data at the current assimilation time. The joint law $\pi_{\mathbf{Y}, \mathbf{X}}$ is specified by the prior marginal $\pi_{\mathbf{X}}$, which corresponds to the forecast distribution, and by the likelihood function $\pi_{\mathbf{Y} | \mathbf{X}}$. For simplicity, we assume that $\pi_{\mathbf{Y}, \mathbf{X}}$ is fully supported on $\mathbb{R}^d \times \mathbb{R}^n$. In filtering, we are only given M samples $\mathbf{x}^1, \dots, \mathbf{x}^M$ from the prior $\pi_{\mathbf{X}}$ —the so-called forecast ensemble—and we wish to sample the posterior (i.e., the filtering distribution)

$$\pi_{\mathbf{X} | \mathbf{y}^*}(\mathbf{x}) = \pi_{\mathbf{X} | \mathbf{Y}}(\mathbf{x} | \mathbf{y}^*) \quad (3.1)$$

for some realization $\mathbf{y}^* \in \mathbb{R}^d$ of the data.

A possible approach to posterior sampling is to construct a *coupling* between prior and posterior distributions using a transformation T such that $\mathbf{Z} := T(\mathbf{X})$ follows the posterior law [76]. This transformation and the associated coupling may or may not be deterministic.

In a deterministic coupling, $\mathbf{Z} = T(\mathbf{X})$ for some deterministic transformation $T : \mathbb{R}^n \rightarrow \mathbb{R}^n$ called a *transport map*. In this case, we say that T pushes forward the prior to the

posterior distribution. For any $\mathbf{X} \sim \pi_{\mathbf{X}}$ and map T , the pushforward of $\pi_{\mathbf{X}}$ by T is given by the law of $T(\mathbf{X})$ and is denoted by $T_{\#}\pi_{\mathbf{X}}$. The existence of a map T such that $T(\mathbf{X}) \sim \pi_{\mathbf{X}|\mathbf{y}^*}$ is guaranteed under very mild conditions. For instance, it suffices to have a prior distribution without atoms [76]. In fact, there are infinitely many ways to push forward one distribution to another, some of which minimize a notion of integrated cost. Monge’s optimal map, for example, minimizes the Euclidean L_2 cost $\mathbb{E}[\|T(\mathbf{X}) - \mathbf{X}\|^2]$ over all admissible transformations [54]. Transport maps are interesting because they enable direct posterior sampling. That is, if $\mathbf{x}^1, \dots, \mathbf{x}^M$ are i.i.d. samples from the prior, then $T(\mathbf{x}^1), \dots, T(\mathbf{x}^M)$ are also i.i.d. samples from the posterior (cf. Figure 3). We will see in Section 3.7 that deterministic couplings are associated with nonlinear generalizations of the square-root EnKF [73].

Remark 1 (Ensemble transform particle filter). *In his pioneering approach to filtering [63], Reich proposes a nonparametric estimator for Monge’s map, by solving the Kantorovich relaxation of a discrete optimal transport problem between the empirical measure given by the prior ensemble and the empirical approximation of the posterior distribution obtained by reweighting prior particles according to their likelihood. In this paper, we consider continuous rather than discrete transport, and look for prior-to-posterior transformations—not necessarily optimal with respect to any cost—that can be estimated without resorting to importance sampling, thus avoiding the root cause of particle degeneracy.*

A coupling need not be deterministic. For instance, we can have $\mathbf{Z} = T(\boldsymbol{\Xi}, \mathbf{X}) \sim \pi_{\mathbf{X}|\mathbf{y}^*}$ for some deterministic transformation T and additional random variable $\boldsymbol{\Xi}$. As a function of \mathbf{X} alone, we can think of T as a “stochastic” map. In this work, we consider non-deterministic couplings induced by a map $T : \mathbb{R}^d \times \mathbb{R}^n \rightarrow \mathbb{R}^n$ such that $\mathbf{Z} = T(\mathbf{Y}, \mathbf{X})$, where \mathbf{Y} represents the data random variable of the Bayesian inference problem. These couplings can be used for posterior sampling like their deterministic counterpart: if $(\mathbf{y}^1, \mathbf{x}^1), \dots, (\mathbf{y}^M, \mathbf{x}^M)$ are i.i.d. samples from the joint distribution $\pi_{\mathbf{Y}, \mathbf{X}}$, then $T(\mathbf{y}^1, \mathbf{x}^1), \dots, T(\mathbf{y}^M, \mathbf{x}^M)$ are also i.i.d. samples from the posterior. In fact, the transformation T is a transport map that pushes forward $\pi_{\mathbf{Y}, \mathbf{X}}$ to the posterior. Inference with non-deterministic couplings is interesting because we can build estimators for T using only *convex* optimization. We will see in Section 3.3 that non-deterministic couplings are linked to nonlinear generalizations of the stochastic EnKF [15].

There is no unique way to couple prior and posterior distributions in a Bayesian inference problem. In the context of filtering, we need couplings that can be estimated efficiently in high dimensions from finitely many prior samples. In Sections 3.3 and 3.7, we discuss specific choices for these couplings, which lead to novel nonlinear filtering algorithms. Before that, however, we need to discuss the properties of an important transport for our analysis, the Knothe–Rosenblatt rearrangement [66].

3.2. Knothe–Rosenblatt rearrangement

Given any pair of positive densities π, η on \mathbb{R}^n , there exists a unique monotone triangular transport map S —called the Knothe–Rosenblatt (KR) rearrangement—that pushes forward

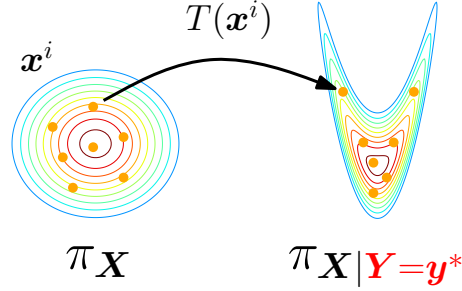


Fig 3: Illustration of a transport map T that pushes forward the prior $\pi_{\mathbf{X}}$ to the posterior $\pi_{\mathbf{X}|\mathbf{Y}=\mathbf{y}^*}$. By the definition of T , if (\mathbf{x}^i) are i.i.d. samples from $\pi_{\mathbf{X}}$, then $(T(\mathbf{x}^i))$ are also i.i.d. samples from $\pi_{\mathbf{X}|\mathbf{Y}=\mathbf{y}^*}$.

one of the corresponding distributions to the other [11], i.e., if $\mathbf{Z} \sim \pi$, then $S(\mathbf{Z}) \sim \eta$. A (lower) triangular map $S: \mathbb{R}^n \rightarrow \mathbb{R}^n$ is a multivariate function whose k th component, S^k , depends only on the first k input variables, i.e.,

$$S(\mathbf{z}) = \begin{bmatrix} S^1(z_1) \\ S^2(z_1, z_2) \\ \vdots \\ S^n(z_1, z_2, \dots, z_n) \end{bmatrix}. \quad (3.2)$$

Monotonicity of the multivariate transformation is intended with respect to the lexicographic order on \mathbb{R}^n , which is equivalent to each slice

$$\xi \mapsto S^k(z_1, \dots, z_{k-1}, \xi) \quad (3.3)$$

being an increasing function. For $\pi, \eta > 0$, each function (3.3) is also strictly increasing and the KR rearrangement becomes an invertible map. The existence of the KR rearrangement stem from intuitive factorization properties of any density, e.g., if $\mathbf{Z} = (Z_1, \dots, Z_n) \sim \pi$, then $\pi = \prod_k \pi_{Z_k|\mathbf{Z}_{1:k-1}}$. In fact, perhaps the most important property for our analysis is that the rearrangement provides an implicit characterization of the marginal conditionals of π , whenever $\eta = \mathcal{N}(\mathbf{0}, \mathbf{I}_n)$. In this case, one can show that each one dimensional mapping (3.3) pushes forward the marginal conditional $\xi \mapsto \pi_{Z_k|\mathbf{Z}_{1:k-1}}(\xi|\mathbf{z}_{1:k-1})$ to a one dimensional standard normal, for all $\mathbf{z}_{1:k-1} \in \mathbb{R}^{k-1}$ [68]. We leverage this property in the next section, where we discuss our first filtering algorithm, while we defer questions pertaining to the estimation of the rearrangement to Section 3.4.

3.3. Stochastic map filter

In this section, we outline an algorithm to carry out the analysis step at a given observation time, based on the construction of non-deterministic couplings between forecast and filtering distributions. We refer to the notation of Section 3.1 for an abstract Bayesian inverse problem.

Our goal is to find a map $T : \mathbb{R}^d \times \mathbb{R}^n \rightarrow \mathbb{R}^n$ such that $T(\mathbf{Y}, \mathbf{X}) \sim \pi_{\mathbf{X}|\mathbf{y}^*}$. If we had such a map, then we could easily sample the posterior $\pi_{\mathbf{X}|\mathbf{y}^*}$ by pushing forward samples from the joint distribution $\pi_{\mathbf{Y}, \mathbf{X}}$ through T . See Figure 4 for an illustration. Samples from $\pi_{\mathbf{Y}, \mathbf{X}}$ are also easy to obtain: given a collection of prior (or forecast) samples $(\mathbf{x}^i) \sim \pi_{\mathbf{X}}$, let \mathbf{y}^i be a sample from $\pi_{\mathbf{Y}|\mathbf{X}}(\cdot|\mathbf{x}^i)$, for all $i = 1, \dots, M$. The resulting pairs $(\mathbf{y}^i, \mathbf{x}^i)$ define samples from $\pi_{\mathbf{Y}, \mathbf{X}}$. We are then left with the problem of finding a suitable T . We call T the “analysis” map.

Let S be the KR rearrangement that pushes forward $\pi_{\mathbf{Y}, \mathbf{X}}$ to $\mathcal{N}(\mathbf{0}, \mathbf{I}_{d+n})$. Since the rearrangement is a triangular map, we can always partition it as

$$S(\mathbf{y}, \mathbf{x}) = \begin{bmatrix} S^{\mathcal{Y}}(\mathbf{y}) \\ S^{\mathcal{X}}(\mathbf{y}, \mathbf{x}) \end{bmatrix} \quad (3.4)$$

for some functions $S^{\mathcal{Y}} : \mathbb{R}^d \rightarrow \mathbb{R}^d$ and $S^{\mathcal{X}} : \mathbb{R}^d \times \mathbb{R}^n \rightarrow \mathbb{R}^n$, where $\mathbf{y} \in \mathbb{R}^d$ and $\mathbf{x} \in \mathbb{R}^n$. By the definition of KR rearrangement, we have that the function $S^{\mathcal{X}}$ pushes forward $\pi_{\mathbf{Y}, \mathbf{X}}$ to a standard normal on \mathbb{R}^n , i.e.,

$$S^{\mathcal{X}}(\mathbf{Y}, \mathbf{X}) \sim \mathcal{N}(\mathbf{0}, \mathbf{I}_n). \quad (3.5)$$

Moreover, since the KR rearrangement implicitly characterizes the conditionals of $\pi_{\mathbf{X}, \mathbf{Y}}$ (cf. Section 3.2), we have that the map $\boldsymbol{\xi} \mapsto S^{\mathcal{X}}(\mathbf{y}^*, \boldsymbol{\xi})$ —obtained by fixing the first input of $S^{\mathcal{X}}$ to the observation $\mathbf{y}^* \in \mathbb{R}^d$ —pushes forward the posterior $\pi_{\mathbf{X}|\mathbf{y}^*}$ to $\mathcal{N}(\mathbf{0}, \mathbf{I}_n)$. By combining these properties, we arrive at a definition for the analysis map T as

$$T := S^{\mathcal{X}}(\mathbf{y}^*, \cdot)^{-1} \circ S^{\mathcal{X}}, \quad (3.6)$$

where $S^{\mathcal{X}}(\mathbf{y}^*, \cdot)^{-1}$ denotes the inverse function of the mapping $\boldsymbol{\xi} \mapsto S^{\mathcal{X}}(\mathbf{y}^*, \boldsymbol{\xi})$. Inverting a triangular map is a computationally trivial task, since it reduces to a sequence of one-dimensional root findings. See Algorithm 1 for details. It is immediate to verify that the map T defined in (3.6) pushes forward $\pi_{\mathbf{Y}, \mathbf{X}}$ to $\pi_{\mathbf{X}|\mathbf{y}^*}$, and thus defines a non-deterministic coupling between prior and posterior distributions.

In practice, we need to build an estimator, \hat{T} , for T . We propose to use

$$\hat{T} := \hat{S}^{\mathcal{X}}(\mathbf{y}^*, \cdot)^{-1} \circ \hat{S}^{\mathcal{X}}, \quad (3.7)$$

where we replace S in (3.6) by a constrained maximum likelihood estimator \hat{S} . We describe this estimator in Section 3.4. It turns out that the components of \hat{S} can be computed quickly—in parallel, and via *convex* optimization—from a collection of samples $(\mathbf{y}^i, \mathbf{x}^i) \sim \pi_{\mathbf{Y}, \mathbf{X}}$.

We summarize the resulting analysis step with stochastic maps in Algorithm 2. The term stochastic maps refers to the use of non-deterministic couplings between forecast and filtering distributions.

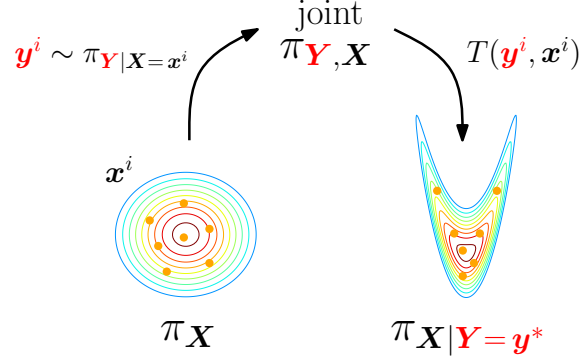


Fig 4: Illustration of the analysis step in the stochastic map filter. For each prior particle \mathbf{x}^i , we generate a sample \mathbf{y}^i from the likelihood function $\pi_{\mathbf{Y}|\mathbf{X}}(\cdot|\mathbf{x}^i)$. The pairs $(\mathbf{y}^i, \mathbf{x}^i)$ represent i.i.d. samples from the joint distribution $\pi_{\mathbf{Y},\mathbf{X}}$ and are used to estimate a transport map T that pushes forward $\pi_{\mathbf{Y},\mathbf{X}}$ to the posterior $\pi_{\mathbf{X}|\mathbf{Y}=\mathbf{y}^*}$. By the definition of T , $(T(\mathbf{y}^i, \mathbf{x}^i))$ gives the desired samples from the posterior distribution.

Algorithm 1 (Invert a triangular map)

Given a map S of the form (3.2) and an $\mathbf{x} \in \mathbb{R}^n$, solve the nonlinear system $S(\mathbf{z}) = \mathbf{x}$ for \mathbf{z} .

- 1: **procedure** INVERTMAP(S, \mathbf{x})
 - 2: **for** $k \leftarrow 1$ to n **do**
 - 3: $z_k \leftarrow$ Solve $S^k(z_1, \dots, z_{k-1}, \xi) = x_k$ for $\xi \in \mathbb{R}$ \triangleright one-dimensional root finding [60]
 - 4: **return** $\mathbf{z} = (z_1, \dots, z_n)$
-

3.4. Estimation of the Knothe–Rosenblatt rearrangement from samples

In this section, we address the estimation of a KR rearrangement S that pushes forward an arbitrary density π on \mathbb{R}^n to a standard normal $\eta = \mathcal{N}(\mathbf{0}, \mathbf{I}_n)$, given only M samples $\mathbf{z}^1, \dots, \mathbf{z}^M$ from π . This problem is at the heart of the filtering methodologies proposed in this paper. For instance, in the stochastic map algorithm of Section 3.3, we need to estimate a KR rearrangement that pushes forward the joint distribution of state and data, $\pi_{\mathbf{X},\mathbf{Y}}$, to a standard normal. In that case, $\mathbf{z}^1, \dots, \mathbf{z}^M$ represent samples from $\pi_{\mathbf{X},\mathbf{Y}}$.

We recall a construction first proposed by [58]. We can build a constrained maximum likelihood estimator for S as follows: let \mathcal{H} be a finite dimensional approximation space for the KR rearrangement, i.e., let \mathcal{H} be a cone of monotone triangular maps $U : \mathbb{R}^n \rightarrow \mathbb{R}^n$ that can be described with finitely many parameters. For each U in \mathcal{H} consider the density given by pulling back η by U , defined as $U^\# \eta := (U^{-1})_\# \eta$ and given explicitly by

$$U^\# \eta(\mathbf{z}) = \eta(U(\mathbf{z})) \det \nabla U(\mathbf{z}), \quad (3.8)$$

where $\det \nabla U$ denotes the determinant of the gradient of the map. Note that π can be written as $S^\# \eta$ by the definition of the KR rearrangement S . Thus, the family of densities $(U^\# \eta)_{U \in \mathcal{H}}$ defines a parametric model for π —the law of the samples $\mathbf{z}^1, \dots, \mathbf{z}^M$. A

Algorithm 2 (Analysis step with stochastic maps)

Given M samples $\mathbf{x}^1, \dots, \mathbf{x}^M$ from the forecast distribution, a likelihood function $\pi_{\mathbf{Y}|\mathbf{X}}$, and an observation \mathbf{y}^* , generate a particle approximation $\mathbf{z}^1, \dots, \mathbf{z}^M$ of the filtering distribution $\pi_{\mathbf{X}|\mathbf{y}^*}$.

```

1: procedure ANALYSISSTOCHASTIC(  $\mathbf{y}^*$ ,  $\pi_{\mathbf{Y}|\mathbf{X}}$ ,  $\mathbf{x}^1, \dots, \mathbf{x}^M$  )
2:   for  $i \leftarrow 1$  to  $M$  do                                     ▷ Generate samples from  $\pi_{\mathbf{Y},\mathbf{X}}$ 
3:      $\mathbf{y}^i \leftarrow$  sample from  $\pi_{\mathbf{Y}|\mathbf{X}}(\cdot|\mathbf{x}^i)$ 
4:      $\widehat{S}^{\mathbf{x}} \leftarrow$  estimator of  $S^{\mathbf{x}}$  from  $(\mathbf{y}^i, \mathbf{x}^i)_{i=1}^M$  given by (3.9).  $S^{\mathbf{x}}$  is defined in (3.4)
5:     for  $i \leftarrow 1$  to  $M$  do                                     ▷ Action of  $\widehat{T}$  as defined in (3.7)
6:        $\mathbf{z}^i \leftarrow \widehat{S}^{\mathbf{x}}(\mathbf{y}^i, \mathbf{x}^i)$ 
7:        $\mathbf{z}^i \leftarrow \text{INVERTMAP}(\widehat{S}^{\mathbf{x}}(\mathbf{y}^*, \cdot), \mathbf{z}^i)$ 
8:   return  $\mathbf{z}^1, \dots, \mathbf{z}^M$ 

```

maximum likelihood estimator, \widehat{S} , for S can then be written as

$$\widehat{S} \in \arg \max_{U \in \mathcal{H}} \frac{1}{M} \sum_{i=1}^M \log U^\# \eta(\mathbf{z}^i). \quad (3.9)$$

Indeed, $\widehat{S}^\# \eta$ minimizes an empirical estimate of the Kullback–Leibler divergence between π and the class of densities given by (3.8) for $U \in \mathcal{H}$.

Since $\eta = \mathcal{N}(\mathbf{0}, \mathbf{I}_n)$, a simple calculation shows that each component, \widehat{S}^k , of \widehat{S} can be computed independently as [58]

$$\widehat{S}^k \in \arg \min_{U^k \in \mathcal{H}_k} \frac{1}{M} \sum_{i=1}^M \left(\frac{1}{2} U^k(\mathbf{z}^i)^2 - \log \partial_k U^k(\mathbf{z}^i) \right), \quad (3.10)$$

where \mathcal{H}_k is a function space for the k th component, U^k , of $U \in \mathcal{H}$, and where $\partial_k U^k$ denotes the derivative of U^k with respect to its k th input variable. \mathcal{H}_k contains functions $U^k : \mathbb{R}^k \rightarrow \mathbb{R}$ that are monotone with respect to the last input variable, i.e., where each $\xi \mapsto U^k(z_1, \dots, z_{k-1}, \xi)$ is an increasing map.

In practice, we need to pick a parameterization for U^k in (3.10), i.e., we need to specify a choice for \mathcal{H}_k . Different choices lead to different filtering algorithms (cf. Algorithm 2). For instance, if we restrict \mathcal{H}_k to contain only affine maps—i.e., $U^k(\mathbf{z}) = u_0 + \sum_{i \leq k} u_i z_i$ for some unknown coefficients (u_i) —then we obtain an EnKF-type algorithm. (We clarify this connection in Section 3.6.) If we depart from the linear ansatz, however, we obtain a whole new class of nonlinear filtering algorithms. For example, in this paper we experiment with *separable* parameterizations of the form $U^k(\mathbf{z}) = \sum_{i \leq k} \mathbf{u}_i(z_i)$ for some collection of nonlinear functions (\mathbf{u}_i) ,

$$\mathbf{u}_i(z) = \sum_j u_{ij} \psi_j(z), \quad (3.11)$$

which can be expressed in terms of finitely many basis functions (ψ_j)—e.g., Hermite polynomials or radial basis functions—and unknown coefficients (u_{ij}). These parameterizations are perhaps the simplest way to increase complexity with respect to a linear function, and lead to filtering algorithms that can outperform the EnKF in several challenging scenarios, with only a marginal increase in computational cost (see Section 4). We describe separable parameterizations in Appendix A, together with a general way to represent monotone triangular maps.

For the parameterizations that we consider in this paper, (3.10) is a finite-dimensional convex program that can be solved efficiently—even in high dimensions—via standard convex optimization methods (e.g., Newton’s method). If we make certain structural assumptions on the estimator, however, (3.10) admits a closed form solution without any need for numerical optimization. For instance, if we let $U^k(\mathbf{z}) = \mathbf{u}(z_1, \dots, z_{k-1}) + \mathbf{u}_k(z_k)$ for some nonlinear function \mathbf{u} and affine \mathbf{u}_k , then (3.10) reduces to a standard *linear regression* problem, provided that we consider parameterizations of \mathbf{u} that are linear in the unknown coefficients. We refer to Appendix A for additional details on this topic.

3.5. Regularization in high dimensions: localization of nonlinear maps

In this section, we discuss how to regularize the estimation of the KR rearrangement S in high dimensions, by imposing certain functional constraints—e.g., sparsity—on the structure of the maximum likelihood estimator \hat{S} defined in (3.9). Regularization is the cornerstone of filtering algorithms that aim to work in high dimensions with a limited ensemble size: examples include covariance tapering and inflation in the EnKF, or weight localization in particle filters [26, 59]. In this work, we do not regularize the estimation of a covariance matrix, but rather the estimation of a more general nonlinear function: the KR rearrangement S .

Like every estimator, \hat{S} has a bias—which quantifies how well we can approximate the true KR rearrangement in the limit of infinite data—and a variance—which measures the variability of the estimate with respect to different realizations of the samples $\mathbf{z}^1, \dots, \mathbf{z}^M$ from π . Both bias and variance of \hat{S} —which is a random function—can be controlled by changing the complexity of the approximation space for the estimator. Very rich parameterizations can yield estimators with low bias, but potentially unacceptable variance, if the number of samples $\mathbf{z}^1, \dots, \mathbf{z}^M$ is insufficient. There is no point in trying to learn arbitrarily nonlinear transformations. In fact, that would be harmful. On the other hand, overly simple parameterizations that can be fitted with low variance might have an unnecessarily large estimation bias, leading to a waste of computational resources. Successful estimation requires addressing this bias-variance tradeoff, especially when dealing with high dimensions and low ensemble regimes.

There are many ways to regularize the estimation of the KR rearrangement. For instance, one could augment the average log-likelihood in (3.9) with a convex penalty on the coefficients of \hat{S} —e.g., a ridge or lasso functional [31]—yielding a penalized maximum likelihood estimator. In addition, one could constrain the function space for the estimator by using

only low-order nonlinear basis functions (see Appendix A). In this section, we focus on the complementary idea of regularizing the estimation by imposing *sparsity* constraints on \widehat{S} , i.e., by dropping some variable dependence from each component of the map, such that

$$\widehat{S}^k(z_1, \dots, z_k) = \widehat{S}^k(z_{j_1}, \dots, z_{j_q}, z_k) \quad (3.12)$$

for some indices j_1, \dots, j_q and integer $q < k - 1$ [71]—effectively introducing a notion of “localization” for nonlinear transformations. We now discuss model assumptions that justify a sparsity pattern like (3.12).

The sparsity of a KR rearrangement S that pushes forward a density π on \mathbb{R}^n to $\mathcal{N}(\mathbf{0}, \mathbf{I}_n)$ depends on marginal conditional independence properties of π . As explained in [71], if $\mathbf{Z} = (Z_1, \dots, Z_n) \sim \pi$, then the k th component of S is *not* a function of the j th input variable ($j < k$) if Z_j and Z_k are conditionally independent given the remaining variables with index less than k , i.e., if

$$Z_j \perp\!\!\!\perp Z_k \mid \mathbf{Z}_{\{1:k-1\} \setminus j}. \quad (3.13)$$

Whether (3.13) holds, perhaps only approximately, depends on properties of π such as decay of dependence and conditional independence. These properties are fairly common when filtering spatially distributed processes since they encode an intuitive notion of local probabilistic interaction between the random variables [64, 74].

Decay of dependence and banded estimators Let $d(\cdot, \cdot)$ be a distance function on the index set $\{1, \dots, n\}$, which defines a natural ordering of the variables \mathbf{Z} , so that larger values of $d(i, j)$ are associated with a weaker statistical dependence between Z_i and Z_j . For instance, in data assimilation $d(\cdot, \cdot)$ could be derived from a metric in physical space. The first observation is that the k th component of the KR rearrangement should depend *weakly* on variables that are far away from Z_k , according to $d(\cdot, \cdot)$. To exploit this structure, let $\mathcal{A}_{k,r}$ denote the set of indices of state variables that are within a distance r from Z_k , i.e.,

$$\mathcal{A}_{k,r} := \{i \in (1, \dots, k) \text{ s.t. } d(i, k) \leq r\}. \quad (3.14)$$

We propose to build an estimator \widehat{S} of S for which each component \widehat{S}^k depends only on the variables in $\mathcal{A}_{k,r}$,

$$\widehat{S}(\mathbf{z}) = \begin{bmatrix} \widehat{S}^1(\mathbf{z}_{\mathcal{A}_{1,r}}) \\ \vdots \\ \widehat{S}^n(\mathbf{z}_{\mathcal{A}_{n,r}}) \end{bmatrix}, \quad (3.15)$$

for an “optimal” value of $r \geq 0$. This r is obtained by minimizing some prediction metric (e.g., RMSE) in an offline calibration phase, as if it were the optimal localization radius for the EnKF [26].

In the case of linear maps, (3.15) corresponds to a “banded” estimator for the Cholesky factor of the precision matrix of the ensemble $\mathbf{z}^1, \dots, \mathbf{z}^M$ [79, 9], and has been used for the purpose of regularized covariance estimation in the context of data assimilation [57]. Indeed, if $\pi = \mathcal{N}(\mathbf{0}, \boldsymbol{\Sigma})$ and $\boldsymbol{\Sigma} = \mathbf{L}\mathbf{L}^\top$ is a Cholesky decomposition of $\boldsymbol{\Sigma} \succ 0$, then $\mathbf{S} := \mathbf{L}^{-1}$

represents a *linear* KR rearrangement that pushes forward π to a standard normal. In this paper, we extend these banded estimators to the nonlinear/non-Gaussian case, using the KR rearrangement to generalize the notion of a Cholesky factor.

Markov properties and graphical models The sparsity pattern of the estimator \widehat{S} can also be justified on the grounds of conditional independence properties of π —the so-called Markov properties. These properties can be collected in a simple undirected graph $\mathcal{G} = (\mathcal{V}, \mathcal{E})$, where each node $i \in \mathcal{V}$ is associated with one of the random variables in the collection $\mathbf{Z} = (Z_1, \dots, Z_n)$, and where each edge $(i, j) \in \mathcal{E}$ encodes a notion of probabilistic interaction between the pair Z_i, Z_j . We say that \mathbf{Z} (or π) is a Markov random field (MRF) with respect to \mathcal{G} if for any partition $\mathcal{A}, \mathcal{S}, \mathcal{B}$ of the vertex set—for which \mathcal{S} is a separator set⁴ for \mathcal{A} and \mathcal{B} —we have that $\mathbf{Z}_{\mathcal{A}}$ and $\mathbf{Z}_{\mathcal{B}}$ are conditionally independent given $\mathbf{Z}_{\mathcal{S}}$, i.e., $\mathbf{Z}_{\mathcal{A}} \perp\!\!\!\perp \mathbf{Z}_{\mathcal{B}} | \mathbf{Z}_{\mathcal{S}}$ [41]. See Figure 6 (*left*) for an example. For any strictly positive π , we can find the sparsest \mathcal{G} that is compatible with the conditional independence structure of π as follows: let $(i, j) \notin \mathcal{E}$ if and only if $\mathbf{Z}_i \perp\!\!\!\perp \mathbf{Z}_j | \mathbf{Z}_{\mathcal{V} \setminus \{i, j\}}$ [40].

A key result in [71] links the sparsity of the KR rearrangement S to the sparsity of \mathcal{G} . For a given \mathcal{G} , define the sequence of marginal graphs $\mathcal{G}^n, \dots, \mathcal{G}^1$ using a simple recursion: (1) $\mathcal{G}^n := \mathcal{G}$, and (2) \mathcal{G}^{k-1} is obtained from \mathcal{G}^k by removing node k and by turning its neighborhood $\text{Nb}(k, \mathcal{G}^k)$ into a fully connected subset,⁵ i.e., a clique. By [71, Theorem 5.1], each component S^k of the rearrangement can only depend on variables in $\text{Nb}(k, \mathcal{G}^k)$, for all $k = 1, \dots, n$. See Figure 5 for an illustration (adapted from [71]). Hence, if we know that π is Markov with respect to a sparse graph, then we can translate this information into sparsity of the estimator \widehat{S} , possibly increasing the sparsity pattern in (3.15).

If $\pi = \mathcal{N}(\mathbf{0}, \Sigma)$, then describing the sparsity of a linear KR rearrangement due to conditional independence reduces to the problem of characterizing the fill-in for the Cholesky factor of the precision matrix Σ^{-1} —a well-known result in the field of Gaussian graphical models [40], which has also been exploited in the context of data assimilation to devise regularized estimators of the ensemble covariance [74]. Here, we consider the non-Gaussian generalization provided by [71], where the Cholesky factor is replaced by a nonlinear KR rearrangement. In particular, we note that the sparsity of S depends on the ordering of the input variables in the same way as the fill-in of the Cholesky factor does. Different orderings can yield different sparsity patterns. See Figure 6 (*right*) for an example. Whenever possible, we then look for orderings that promote sparsity (cf. [71] for additional details).

In many cases, π is only *approximately* Markov with respect to a sparse graph \mathcal{G} , e.g., there might exist a second density π' which is Markov with respect to \mathcal{G} and such that $\mathcal{D}_{\text{KL}}(\pi' || \pi) < \varepsilon$, for some $\varepsilon > 0$. In particular, we know that the filtering marginals will not be “exactly” Markov with respect to a sparse \mathcal{G} , since conditional independence properties do not persist over time for general models [40]. Yet, when filtering spatially distributed processes (e.g., in data assimilation) it is reasonable to expect that the filtering (or forecast) marginals will be well-approximated by sparse MRFs, since the latter encode probabilis-

⁴ \mathcal{S} is a separator set for \mathcal{A} and \mathcal{B} if every path from a node in \mathcal{A} to a node in \mathcal{B} goes through \mathcal{S} .

⁵For any graph \mathcal{G} , we denote by $\text{Nb}(k, \mathcal{G})$ the neighborhood of a node k in \mathcal{G} .

tic models with local or neighboring interactions. For example, in Section 4 we consider the Lorenz-96 model, which arises from the discretization of a one-dimensional PDE on a periodic domain. In that case, we can expect that the filtering marginal is approximately Markov with respect to a cycle graph with a low-degree of connectivity between the nodes. When dealing with two-dimensional PDEs, it is natural to consider grid graphs [74, 45], or more general lattices on the plane, and so on for higher dimensional domains. In practice, we can then sparsify the estimator \hat{S} according to a graph \mathcal{G} , which implies Markov properties for π that are only approximately satisfied, and treat the exact geometry of the graph—e.g., its neighborhood structure—as a calibration parameter of the algorithm, as if it were a localization radius. This is equivalent to regularizing the estimation of the KR rearrangement by projecting π onto a manifold of sparse MRFs [40].

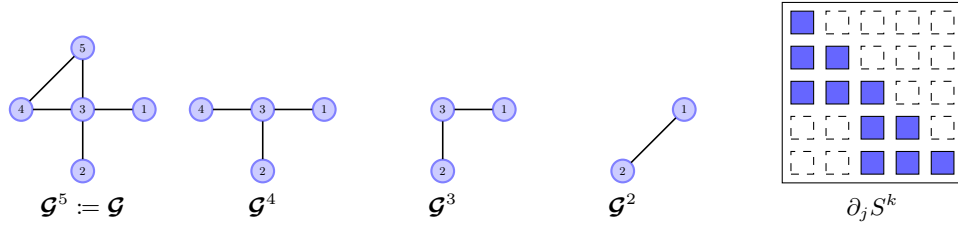


Fig 5: Here, we assume that π is Markov with respect to the leftmost graph \mathcal{G} , and show the sequence of marginal graphs (\mathcal{G}^k) defined in Section 3.5. We then represent the sparsity of the corresponding KR rearrangement S using symbolic matrix notation: the (j, k) -th entry of the matrix is *not* colored if the k th component of the map does not depend on the j th input variable.

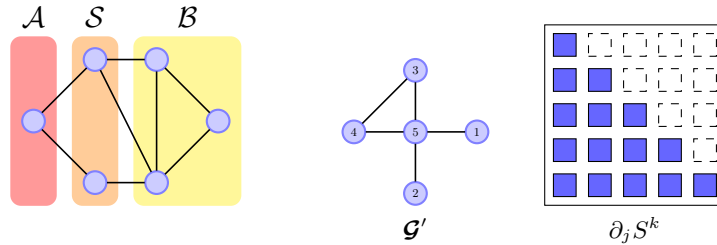


Fig 6: (*left*) Example of a graphical model for \mathcal{Z} , together with a partition $\mathcal{A}, \mathcal{S}, \mathcal{B}$ of the vertex set, where \mathcal{S} is a separator for \mathcal{A} and \mathcal{B} . By definition, $\mathcal{Z}_{\mathcal{A}} \perp\!\!\!\perp \mathcal{Z}_{\mathcal{B}} | \mathcal{Z}_{\mathcal{S}}$. (*center*) Reordering of the input variables for the example of Figure 5, leading to a rearrangement S with no sparsity (*right*).

3.6. Remarks on the stochastic map filter

The stochastic map algorithm of Section 3.3 is a general tool for Bayesian inference: given M samples (\mathbf{x}^i) from the prior, (1) generate M samples $\mathbf{y}^i \sim \pi_{\mathbf{Y}|\mathbf{X}}(\cdot | \mathbf{x}^i)$ from the likelihood,

(2) use the pairs $(\mathbf{y}^i, \mathbf{x}^i)$ to build an estimator \widehat{T} of the analysis map T as

$$T := S^{\mathcal{X}}(\mathbf{y}^*, \cdot)^{-1} \circ S^{\mathcal{X}}, \quad \widehat{T} := \widehat{S}^{\mathcal{X}}(\mathbf{y}^*, \cdot)^{-1} \circ \widehat{S}^{\mathcal{X}}, \quad (3.16)$$

and (3) obtain a particle approximation of the posterior as $\widehat{T}(\mathbf{y}^1, \mathbf{x}^1), \dots, \widehat{T}(\mathbf{y}^M, \mathbf{x}^M)$.

A few remarks are in order. First, we only need to *sample* the likelihood function and do not need explicit access to the density $\pi_{\mathbf{Y}|\mathbf{X}}$, which might be intractable or expensive to evaluate. We are thus in the setting of approximate Bayesian computation (ABC) methods [51] or, more broadly, inference in *generative models*. Second, we can compute \widehat{T} using *convex* optimization: we only need to estimate a few components, $S^{\mathcal{X}}$, of the KR rearrangement S that pushes forward $\pi_{\mathbf{Y},\mathbf{X}}$ to a standard normal, using the constrained maximum likelihood estimator defined in (3.9). In particular, the block $S^{\mathcal{Y}}$ defined in (3.4) is not needed, while the components of $\widehat{S}^{\mathcal{X}}$ can be computed in parallel using (3.10). Third, the estimation of $S^{\mathcal{X}}$ in high dimensions can be regularized using the localization techniques of Section 3.5. (For the purpose of posterior sampling, we may only care about the bias-variance tradeoff in the estimation of T , and not necessarily that of $S^{\mathcal{X}}$.) Fourth, if we constrain the estimator $\widehat{S}^{\mathcal{X}}$ to be linear, then we recover an EnKF with “perturbed observations,” i.e., the stochastic EnKF [15].

Remark 2 (Connection with the EnKF). *Assume that the samples $(\mathbf{y}^i, \mathbf{x}^i)$ have been centered, so that they have zero mean. Then, the best linear estimator of $S^{\mathcal{X}}$ —according to (3.9)—is given by*

$$\widehat{S}^{\mathcal{X}}(\mathbf{y}, \mathbf{x}) = \mathbf{A} \left(\mathbf{x} - \widehat{\Sigma}_{\mathbf{X},\mathbf{Y}} \widehat{\Sigma}_{\mathbf{Y}}^{-1} \mathbf{y} \right), \quad (3.17)$$

where \mathbf{A} is the inverse of the Cholesky factor of the “residual” covariance matrix,

$$\widehat{\Sigma}_{\mathbf{X}|\mathbf{Y}} := \widehat{\Sigma}_{\mathbf{X}} - \widehat{\Sigma}_{\mathbf{X},\mathbf{Y}} \widehat{\Sigma}_{\mathbf{Y}}^{-1} \widehat{\Sigma}_{\mathbf{X},\mathbf{Y}}^{\top}, \quad (3.18)$$

where $\widehat{\Sigma}_{\mathbf{X}}$, $\widehat{\Sigma}_{\mathbf{Y}}$, and $\widehat{\Sigma}_{\mathbf{X},\mathbf{Y}}$ are empirical (maximum likelihood) estimators of $\text{Var}(\mathbf{X})$, $\text{Var}(\mathbf{Y})$, and $\text{Cov}(\mathbf{X}, \mathbf{Y})$, respectively.⁶ For a given observation \mathbf{y}^* of the data, we can then compute a closed form expression for the inverse of the map $\xi \mapsto \widehat{S}^{\mathcal{X}}(\mathbf{y}^*, \xi)$ and for the estimator of the analysis map,

$$\widehat{T}(\mathbf{y}, \mathbf{x}) = \mathbf{x} - \widehat{\Sigma}_{\mathbf{X},\mathbf{Y}} \widehat{\Sigma}_{\mathbf{Y}}^{-1} (\mathbf{y} - \mathbf{y}^*), \quad (3.19)$$

which corresponds to the forecast-to-analysis update of the stochastic EnKF [67]. The stochastic map filter offers a framework to generalize this linear ansatz to more general nonlinear transformations.

At any assimilation time, we need to condition the forecast distribution on d scalar observations $\mathbf{y}^* = (y_1^*, \dots, y_d^*)$ from \mathbf{Y} . In Section 3.3, we presented an algorithm that can

⁶In the case of a linear–Gaussian observation model, e.g., if $\mathbf{Y} = \mathbf{H}\mathbf{X} + \mathcal{E}$ for $\mathcal{E} \sim \mathcal{N}(\mathbf{0}, \mathbf{R})$ independent of \mathbf{X} , and with \mathbf{H} known, we could regularize the estimation of $\text{Cov}(\mathbf{X}, \mathbf{Y})$ and $\text{Var}(\mathbf{Y})$ by letting $\widehat{\Sigma}_{\mathbf{X},\mathbf{Y}} := \widehat{\Sigma}_{\mathbf{X}}\mathbf{H}^{\top}$ and $\widehat{\Sigma}_{\mathbf{Y}} = (\mathbf{H}\widehat{\Sigma}_{\mathbf{X}}\mathbf{H}^{\top} + \mathbf{R})$.

assimilate all these observations simultaneously. A possible alternative if the observations are conditionally independent given the state, i.e.,

$$\pi_{\mathbf{Y}|\mathbf{X}} = \prod_{k=1}^d \pi_{Y_k|\mathbf{X}}, \quad (3.20)$$

is to process each scalar observation y_k^* individually and sequentially by iterating d times over Algorithm 2: the posterior ensemble associated with y_k^* can be used as a prior ensemble when assimilating y_{k+1}^* . Hence, the analysis step can be either performed by computing d analysis maps on \mathbb{R}^{n+1} —each map associated with one scalar observation—or by computing a single map on \mathbb{R}^{n+d} (cf. the EnKF with single versus multiple observations [34]).

Remark 3 (Localize the analysis map for a scalar observation with local likelihood). *When assimilating a scalar observation (or a small batch thereof) it makes sense to consider an additional form of localization for $\widehat{S}^{\mathbf{X}}$ with respect to those already introduced in Section 3.5. The idea is that the analysis map T should revert to the identity function along components that correspond to unobserved variables that are far from the observed ones, for instance with respect to the metric $\mathbf{d}(\cdot, \cdot)$ defined in Section 3.5. We can enforce this identity structure in the estimator \widehat{T} by requiring that some components of $\widehat{S}^{\mathbf{X}}$ be the identity function. Specifically, assume that we are observing a single scalar observation Y which follows a local likelihood model, i.e., $\pi_{Y|\mathbf{X}} = \pi_{Y|X_\ell}$ for some scalar state variable X_ℓ . After a permutation, we can assume that $X_\ell = X_1$ and that the state variables have been reordered in terms of their increasing distance from X_1 . We can then look for an estimator $\widehat{S}^{\mathbf{X}}$ with the following sparsity pattern,⁷*

$$\widehat{S}^{\mathbf{X}}(y, \mathbf{x}) = \begin{bmatrix} s(y, \mathbf{x}_{1:j}) \\ x_{j+1} \\ \vdots \\ x_n \end{bmatrix}, \quad s : \mathbb{R} \times \mathbb{R}^j \rightarrow \mathbb{R}^j, \quad (3.21)$$

for some index j that represents the analogue of a “localization” radius for EnKF algorithms. The effect of (3.21) is to produce an estimator \widehat{T} for the analysis map that reverts to the identity function after j components, thus producing a truly local coupling. Note that the localization in (3.21) is only justified because we use $\widehat{S}^{\mathbf{X}}$ within the expression for \widehat{T} in (3.16). We do not care if $\widehat{S}^{\mathbf{X}}$ is a poor estimator of the rearrangement $S^{\mathbf{X}}$ as a whole, as long as the resulting \widehat{T} given by (3.16) is a good estimator of the analysis map.

Remark 4 (Transform rather than sample). *The estimation of $S^{\mathbf{X}}$ by $\widehat{S}^{\mathbf{X}}$ yields an implicit approximation of the posterior distribution: by definition, the mapping $\boldsymbol{\xi} \mapsto S^{\mathbf{X}}(\mathbf{y}^*, \boldsymbol{\xi})$ pushes forward $\pi_{\mathbf{X}|\mathbf{y}^*}$ to a standard normal. In principle, we could then generate approximate posterior samples by pushing forward samples from a standard normal $\mathcal{N}(\mathbf{0}, \mathbf{I}_n)$ through the inverse of the map $\boldsymbol{\xi} \mapsto \widehat{S}^{\mathbf{X}}(\mathbf{y}^*, \boldsymbol{\xi})$. In practice, however, we do not do this;*

⁷One can easily increase this sparsity pattern using the localization ideas of Section 3.5.

rather, we use $\widehat{S}^{\mathbf{X}}$ to build an estimator \widehat{T} of the prior-to-posterior update. This is in analogy with the EnKF, where the posterior ensemble is given by a (linear) transformation applied to the prior ensemble, rather than by samples from a Gaussian approximation of the posterior.

In numerical experiments—where transformations can only be approximate—we observe that pushing forward samples from $\pi_{\mathbf{Y}, \mathbf{X}}$ through \widehat{T} often yields far more accurate posterior approximations than pushing standard normal samples through $\widehat{S}^{\mathbf{X}}(\mathbf{y}^*, \cdot)^{-1}$. This improvement can be attributed to the cancellation of errors in the composition of $\widehat{S}^{\mathbf{X}}$ with its partial inverse. As a limiting but nonetheless illustrative example: when the data are uninformative and $S^{\mathbf{X}}$ does not depend on \mathbf{y} , the Gaussian samples mapped through the inverse of the estimated map will be affected by bias and variance in $\widehat{S}^{\mathbf{X}}$, while \widehat{T} will be the identity function and generate exact posterior samples. More generally, consider any map $\widehat{S}^{\mathbf{X}}$ that renders $\mathbf{Z} = \widehat{S}^{\mathbf{X}}(\mathbf{Y}, \mathbf{X})$ independent of \mathbf{Y} ; one can show that the transformation \widehat{T} built from this map will again generate exact posterior samples.

We conclude this section with a final remark. We presented the stochastic map filter using the KR rearrangement as our building-block coupling, because the latter can be easily approximated in high dimensions using nonlinear transformations and convex optimization. Yet the algorithm would still make sense if we were to replace the KR rearrangement with any other transport map S that has the “block” structure in (3.4), and that pushes forward $\pi_{\mathbf{Y}, \mathbf{X}}$ to $\mathcal{N}(\mathbf{0}, \mathbf{I}_{d+n})$.

3.7. Deterministic map filter

In this section, we explore the use of deterministic couplings in the analysis step of Section 3.1. In particular, we seek a transport map $T : \mathbb{R}^n \rightarrow \mathbb{R}^n$ that pushes forward prior to posterior, i.e., such that $T(\mathbf{X}) \sim \pi_{\mathbf{X}|\mathbf{y}^*}$. See Figure 3 for an illustration. (Note that in the stochastic map filter of Section 3.3, the map T was defined on \mathbb{R}^{n+d} rather than on \mathbb{R}^n .)

For all monotone triangular maps U on \mathbb{R}^n , define π_U to be the density that is proportional to the function $\boldsymbol{\xi} \mapsto \pi_{\mathbf{Y}|\mathbf{X}}(\mathbf{y}^*|\boldsymbol{\xi}) U^\sharp \eta(\boldsymbol{\xi})$, which is the product of the likelihood and the pullback density $U^\sharp \eta$. Now, let S be the KR rearrangement that pushes forward the prior $\pi_{\mathbf{X}}$ to $\eta := \mathcal{N}(\mathbf{0}, \mathbf{I}_n)$. Hence, the pullback density of η by S —see the definition in (3.8)—is the prior, i.e., $S^\sharp \eta = \pi_{\mathbf{X}}$. It follows that π_S is the posterior density $\pi_{\mathbf{X}|\mathbf{y}^*}$.

We define a candidate analysis map T as follows:

$$T := \mathcal{T} \circ S, \tag{3.22}$$

where \mathcal{T} is a KR rearrangement that pushes forward η to π_S . It is immediate to verify that (3.22) pushes forward $\pi_{\mathbf{X}}$ to $\pi_{\mathbf{X}|\mathbf{y}^*}$, and thus defines a valid deterministic coupling between the prior and posterior distributions.

We propose to estimate T by

$$\widehat{T} := \widehat{\mathcal{T}} \circ \widehat{S}, \tag{3.23}$$

where \widehat{S} and \widehat{T} are (constrained) maximum likelihood estimators of two different KR rearrangements: the former pushes forward $\pi_{\mathbf{X}}$ to η , while the latter pushes forward η to $\pi_{\widehat{S}}$. Intuitively, $\pi_{\widehat{S}}$ is an approximation of the posterior distribution, which depends on the estimator \widehat{S} . We can compute \widehat{S} efficiently via convex optimization from a collection of prior samples $(\mathbf{x}^i) \sim \pi_{\mathbf{X}}$ using the construction of Section 3.4 and the regularization techniques of Section 3.5. The computation of \widehat{T} , however, is less straightforward, as we explain in the next remark. In particular, note that we do not have samples from $\pi_{\widehat{S}}$; instead, given \widehat{S} , we can only evaluate this density up to a normalizing constant, as long as the likelihood $\pi_{\mathbf{Y}|\mathbf{X}}(\mathbf{y}^*|\cdot)$ can be evaluated explicitly.

Remark 5 (Estimation of the Knothe–Rosenblatt rearrangement from densities). \widehat{T} is a maximum likelihood estimator of a KR rearrangement that pushes forward a standard normal $\mathcal{N}(\mathbf{0}, \mathbf{I}_n)$ to a density $\pi := \pi_{\widehat{S}}$ on \mathbb{R}^n , i.e., \widehat{T} is defined analogously to (3.9) as

$$\widehat{T} \in \arg \max_{U \in \mathcal{H}} \frac{1}{N} \sum_{i=1}^N \log U^\# \pi(\mathbf{z}^i), \quad (3.24)$$

for a collection of N samples $(\mathbf{z}^i)_{i=1}^N$ from $\mathcal{N}(\mathbf{0}, \mathbf{I}_n)$ and for some approximation space \mathcal{H} . There is an important difference between (3.9) and (3.24): the density η in (3.9) is always log-concave, while π in (3.24) need not be. As a result, (3.24) is in general not a convex problem [39]. Moreover, we cannot compute the components of \widehat{T} independently as in (3.10), since π need not factorize as a product of its marginals. Hence, the computation of \widehat{T} is inherently harder than that of \widehat{S} , but still feasible. The numerical solution of (3.24) in the context of Bayesian inference was pioneered by [56], which uses gradient-based optimization (e.g., BFGS or Newton-CG [78]) to minimize an equivalent reformulation of (3.24),

$$\widehat{T} \in \arg \min_{U \in \mathcal{H}} -\frac{1}{N} \sum_{i=1}^N \left(\log \pi(U(\mathbf{z}^i)) + \sum_{k=1}^n \log \partial_k U^k(\mathbf{z}^i) \right), \quad (3.25)$$

over a finite dimensional space of polynomial maps (see Appendix A and [52, 10]). Three aspects of (3.25) are particularly important. First, we only need to evaluate $\pi_{\widehat{S}}$ up to a normalizing constant. Second, the number N of samples from $\mathcal{N}(\mathbf{0}, \mathbf{I}_n)$ need not be limited by the cardinality of the forecast ensemble, in contrast to (3.9). Third, we must evaluate the likelihood function $\pi_{\mathbf{Y}|\mathbf{X}}$ for each sample in (3.25). The latter is a crucial contrast with the stochastic map filter of Section 3.3, which only requires sampling from (i.e., simulating) the likelihood.

In the special case of a Gaussian likelihood $\pi_{\mathbf{Y}|\mathbf{X}}$ and linear \widehat{S} , the estimator $\pi_{\widehat{S}}$ of the posterior distribution becomes Gaussian. The corresponding KR rearrangement that pushes forward $\mathcal{N}(\mathbf{0}, \mathbf{I}_n)$ to $\pi_{\widehat{S}}$ is *linear*, meaning that without loss of generality we can solve (3.25) over the space of linear maps. In this case, (3.25) is a convex (quadratic) problem with a closed form expression for \widehat{T} , and the deterministic map filter reduces to a particular ensemble square-root filter [73].

If either $\pi_{\mathbf{Y}|\mathbf{X}}$ is non-Gaussian or \widehat{S} is nonlinear—e.g., if we seek a non-Gaussian approximation of the prior distribution—then the linear ansatz for $\widehat{\mathcal{T}}$ is no longer optimal. In such cases, we might want to capture non-Gaussian structure by considering parameterizations of $\widehat{\mathcal{T}}$ that depart gradually and incrementally from that of a linear function, seeking a balance between accuracy and computational cost (see Section 3.4). In particular, we can regularize the estimation of the rearrangement in high dimensions using localization ideas similar⁸ to those of Section 3.5. We propose to use a “banded” estimator analogous to (3.15) to leverage decay of dependence in π , i.e.,

$$\widehat{\mathcal{T}}(\mathbf{z}) = \begin{bmatrix} \widehat{\mathcal{T}}^1(\mathbf{z}_{\mathcal{A}_{1,r}}) \\ \vdots \\ \widehat{\mathcal{T}}^n(\mathbf{z}_{\mathcal{A}_{n,r}}) \end{bmatrix}, \quad (3.26)$$

for some value of the localization radius $r \geq 0$. For a Gaussian π , (3.26) corresponds to a banded estimator for the Cholesky factor of the *covariance* matrix of π , rather than its precision (cf. Section 3.5).

We summarize the analysis step with deterministic maps in Algorithm 3. Note that there are many possible variations for the definition of the prior-to-posterior update (3.22). Most notably, $\widehat{\mathcal{T}}$ need not approximate a KR rearrangement: in fact any map that pushes forward η to π_S would work, e.g., maps induced by the flows of ODEs [20, 3, 32] or by the composition of many simple functions [46, 22], including deep neural networks [65].

Remark 6 (Connection with the variational mapping particle filter). *The variational mapping particle filter [61] uses the nonparametric variational inference algorithm proposed by [46] to generate approximate samples from a non-Gaussian approximation of the filtering distribution. The idea is to minimize precisely (3.24)—a non-convex functional—by implementing a form of functional gradient descent on a reproducing kernel Hilbert space (RKHS) of transformations (with no restrictions to triangular maps). The non-Gaussian approximation of the unnormalized filtering distribution is defined by the product of the likelihood function with an approximation of the forecast distribution at time k given by⁹*

$$\pi_{\mathbf{Z}_{k+1}|\mathbf{y}_{1:k}} \approx \frac{1}{M} \sum_{i=1}^M \pi_{\mathbf{Z}_{k+1}|\mathbf{Z}_k}(\cdot|\mathbf{z}^i), \quad (3.27)$$

where (\mathbf{z}^i) represent (approximate) samples from the previous filtering marginal $\pi_{\mathbf{Z}_k|\mathbf{y}_{1:k}}$. This approximation of the forecast density contrasts with the regularized maximum likelihood estimation of the KR rearrangement S in (3.22) from the forecast ensemble, using (3.9). Indeed, it would be interesting to approximate the rearrangement $\widehat{\mathcal{T}}$ in the deterministic map algorithm using the technique of [46] (or its second-order extension [22]), after

⁸Most of the discussion of Section 3.5 is specific to a KR rearrangement whose target distribution is a product measure on \mathbb{R}^n —e.g., $\mathcal{N}(\mathbf{0}, \mathbf{I}_n)$ —and thus does not apply to the estimation of \mathcal{T} . See [71] for additional details.

⁹For ease of exposition, we assume that the dynamic of the latent field is only given at the observation times.

“localizing” the RKHS of transformations by imposing a sparsity pattern like the one in (3.26). Regularization is critical in high dimensions.

The deterministic map filter presented in this section features an inherently non-convex step. This is an important distinction from the stochastic map filter of Section 3.3, which relies solely on convex optimization (at the price of computing a higher dimensional transformation). In Appendix B, we discuss a common structural assumption on the state-space model that allows us to easily bypass non-convex optimization in the deterministic map algorithm, leading to a scheme with close ties to the multivariate rank histogram filter [53].

Algorithm 3 (Analysis step with deterministic maps)

Given M samples $\mathbf{x}^1, \dots, \mathbf{x}^M$ from the forecast distribution, a likelihood function $\pi_{\mathbf{Y}|\mathbf{X}}$, and an observation \mathbf{y}^* , generate a particle approximation $\mathbf{z}^1, \dots, \mathbf{z}^M$ of the filtering distribution $\pi_{\mathbf{X}|\mathbf{y}^*}$. Let $\eta := \mathcal{N}(\mathbf{0}, \mathbf{I}_n)$.

```

1: procedure ANALYSISDETERMINISTIC(  $\mathbf{y}^*$ ,  $\pi_{\mathbf{Y}|\mathbf{X}}$ ,  $\mathbf{x}^1, \dots, \mathbf{x}^M$  )
2:    $\hat{S} \leftarrow$  estimator of  $S$  from  $(\mathbf{x}^i)_{i=1}^M$  given by (3.9) ▷  $S_{\#} \pi_{\mathbf{X}} = \eta$ 
3:   Define  $\pi_{\hat{S}}$  as  $\pi_{\hat{S}}(\boldsymbol{\xi}) \propto \pi_{\mathbf{Y}|\mathbf{X}}(\mathbf{y}^*|\boldsymbol{\xi}) \hat{S}_{\#} \eta(\boldsymbol{\xi})$ 
4:    $\hat{\mathcal{T}} \leftarrow$  estimator of  $\mathcal{T}$  from  $\pi_{\hat{S}}$  given by (3.25) ▷  $\hat{\mathcal{T}}_{\#} \eta = \pi_{\hat{S}}$ 
5:   for  $i \leftarrow 1$  to  $M$  do ▷ Action of  $\hat{\mathcal{T}}$  as defined in (3.23)
6:      $\mathbf{z}^i \leftarrow \hat{S}(\mathbf{x}^i)$ 
7:      $\mathbf{z}^i \leftarrow \hat{\mathcal{T}}(\mathbf{z}^i)$ 
8:   return  $\mathbf{z}^1, \dots, \mathbf{z}^M$ 

```

4. Numerical experiments

In this section, we numerically investigate the performance of the stochastic map filter over a range of examples. We show that nonlinear configurations of the new filter can have tracking performance consistently superior to that of the EnKF. We also show that the stochastic map filter provides better approximations of the true (Bayesian) filtering distribution. We focus on the stochastic map filter because it can be implemented using only convex optimization, regardless of any nonlinear/non-Gaussian structure in the state-space model. Numerical experiments with earlier versions of the deterministic map filter can be found in related work by the authors [71, Ch. 6], for the special case of conditionally independent and local observations (see Appendix B). Many aspects of our problem setup and our performance assessment follow [44], as detailed below.

4.1. Common aspects of the problem configurations

First we discuss aspects of the numerical experiments that are shared among the test problems of Sections 4.2–4.3 and Appendix E.

Prior models We consider two dynamical models of increasing dimension: the Lorenz-63 and the Lorenz-96 models, which are widely used testbeds for filtering in chaotic dynamical systems. The Lorenz-63 model is a three-dimensional system introduced in [47] that describes the natural convection of a heated fluid. The state at time t is a three-dimensional vector $\mathbf{Z}(t) = (Z_1(t), Z_2(t), Z_3(t))$ whose dynamics are given by the ODE system,

$$\frac{dZ_1}{dt} = -\sigma Z_1 + \sigma Z_2, \quad \frac{dZ_2}{dt} = -Z_1 Z_3 + \rho Z_1 - Z_2, \quad \frac{dZ_3}{dt} = Z_1 Z_2 - \beta Z_3, \quad (4.1)$$

where (β, ρ, σ) are fixed parameters. In our experiments, we set $\beta = 8/3$, $\rho = 28$, and $\sigma = 10$, which produces chaotic solutions tending to the well-known Lorenz attractor.

The Lorenz-96 model is a popular testbed for numerical weather prediction algorithms, reproducing coarse features of the mid-latitude atmosphere [48, 49]. The state at time t is a 40-dimensional vector, $\mathbf{Z}(t) = (Z_1(t), \dots, Z_{40}(t))$. The state dynamics are defined by a set of nonlinear ODEs that represent the spatial discretization of a time-dependent PDE, i.e.,

$$\frac{dZ_j}{dt} = (Z_{j+1} - Z_{j-2})Z_{j-1} - Z_j + F, \quad j = 1, \dots, 40, \quad (4.2)$$

with periodic boundary conditions and constant forcing parameter F [64]. In our experiments we use $F = 8$, which leads to a fully chaotic dynamic [49].

We integrate both ODE systems, (4.1) and (4.2), using a fourth-order explicit Runge-Kutta method, with constant stepsizes $\Delta t = 0.05$ and $\Delta t = 0.01$, respectively. For the Lorenz-63 model only, we also wish to construct a “reference” Bayesian filtering solution via a consistent formulation of the particle filter. In this case, we add a small amount of Gaussian noise to the state at each integration step, $\boldsymbol{\varepsilon}_{\Delta t} \sim \mathcal{N}(0, 10^{-4}\mathbf{I}_3)$, for the purpose of delaying degeneracy of the particle filter. We note that the EnKF and the stochastic map filter remain stable for the Lorenz-63 configurations below *without* this additive noise. We do not add any noise to the dynamics of the Lorenz-96 model. Therefore, the Markov transition kernel for the Lorenz-96 model is intractable.

Likelihood model The state of each system is observed indirectly every Δt_{obs} time units. Larger values of Δt_{obs} are associated with increasingly non-Gaussian forecast statistics. We index the state at discrete observation times by $(\mathbf{Z}_k)_{k \geq 1}$ where $\mathbf{Z}_k = \mathbf{Z}(k\Delta t_{\text{obs}})$ (e.g., see Figure 1). For any observation step k , the likelihood model is specified by

$$\mathbf{Y}_k = \mathbf{H}\mathbf{Z}_k + \boldsymbol{\varepsilon}_k, \quad (4.3)$$

where $\mathbf{H} \in \mathbb{R}^{d \times n}$ is a linear operator that selects $d \leq n$ components of the state at uniform intervals (e.g., every other component, or every fourth component), while $\boldsymbol{\varepsilon}_k$ is an additive noise that is independent of \mathbf{Z}_k . In Sections 4.2 and 4.3, we consider configurations using Gaussian observational noise with zero mean and covariance $\theta^2\mathbf{I}_d$. In Section E, we employ *heavy-tailed* Laplace observational noise with zero mean and covariance $2\theta^2\mathbf{I}_d$ (i.e., scale parameter θ for each dimension).

Simulation setup Given a random initial condition \mathbf{Z}_0 drawn from $\mathcal{N}(\mathbf{0}, \mathbf{I}_n)$, we generate a sequence of “true” hidden states $(\mathbf{z}_k^*)_k$ and a sequence of synthetic observations $(\mathbf{y}_k^*)_k$, with the same model used for filtering. We are thus in the usual “identical twin experiment” setting [64], wherein the filtering algorithms must estimate the true state given only these synthetic observations. In Appendix D, we depart from this setting to demonstrate robustness of the results to a mismatch between the discretizations of the data-generating model and the model used for filtering.

The initial ensemble for the filtering algorithms is generated through a *spin-up* phase. First, we draw M i.i.d. random samples of the initial condition, $\mathcal{N}(\mathbf{0}, \mathbf{I}_n)$. Then, we run the stochastic EnKF—without localization—for 2000 assimilation steps. Using the resulting ensemble at $k = 2000$, we then apply the filter to be tested (e.g., an EnKF with optimally tuned localization, or the stochastic map filter) for an additional 4000 assimilation steps. At each step, we use the ensemble mean $\bar{\mathbf{z}}_k := \frac{1}{M} \sum_{i=1}^M \mathbf{z}_k^i$ as a point estimate of the true state \mathbf{z}_k^* . Lastly, to eliminate the transient effect of switching between filtering algorithms, we analyze the assimilation quality only using the last 2000 assimilation cycles. We also performed studies with up to 10^4 assimilation cycles in this last phase, but found no significant difference in the results.

Performance metrics We evaluate the tracking performance of the filter via the root-mean-squared error (RMSE), defined at any assimilation step k as $\text{RMSE}_k := \|\bar{\mathbf{z}}_k - \mathbf{z}_k^*\|_2 / \sqrt{n}$. To measure the concentration of the ensemble members, we compute the ensemble spread, defined at any assimilation step k as $[\text{tr}(\widehat{\Sigma}_k)/n]^{1/2}$, where $\widehat{\Sigma}_k$ denotes the ensemble covariance matrix at step k . In Sections 4.2–4.3 and E, we report the *time average* of each of these metrics (e.g., over the 2000 test assimilation steps) as a function of the ensemble size M . In addition, we compute the coverage probability of the intervals given by the empirical 2.5% and 97.5% quantiles of each marginal of the ensemble, i.e., the frequency with which the i th component of \mathbf{z}_k^* is contained in the i th marginal interval. For each component, this frequency is of the form k/T where $k \in \{0, \dots, T\}$ denotes the number of intervals that contain the corresponding component of the true state, and T represents the total number of assimilation times. We then average these coverage probabilities over the n components of the state. Lastly, evaluations of the ensemble quality based on the *continuous ranked probability score* [28] are presented in Appendix C.

Algorithm parameters The results below investigate the performance of the stochastic map filter (Algorithm 2) as nonlinearities are gradually introduced in the prior-to-posterior transformation \widehat{T} .

Each component function U^k of the map $S^{\mathcal{X}}$ is allowed to depend on the data y and on a subset of the state variables z_1, \dots, z_k given by $\mathbf{z}_{\mathcal{A}_{k,r}}$. In particular, our numerical experiments consider a separable representation $U^k(y, \mathbf{z}_{\mathcal{A}_{k,r}}) = \mathbf{u}_0^k(y) + \sum_{i \in \mathcal{A}_{k,r}} \mathbf{u}_i^k(z_i)$ for $k = 1, \dots, n$. For the linear version of the stochastic map filter, labeled as “linear” in the figures, \mathbf{u}_0^k and \mathbf{u}_i^k are restricted to be linear functions. To increase the complexity of the map, we add radial basis functions (RBFs) to the approximation spaces for \mathbf{u}_0^1 , \mathbf{u}_0^k , and \mathbf{u}_i^k for $i < k$. For \mathbf{u}_1^1 , we use a monotone parameterization based on integrals of radial basis

functions (sigmoids), and we keep \mathbf{u}_k^k linear for $k > 1$. See Appendix A for more details on this representation. While many other nonlinear representations of U^k are possible, this particular separable form was chosen because it gradually adds degrees of freedom starting from a linear representation and allows (3.10) to be solved in closed form for $k > 1$. We label results for maps with linear terms plus p RBFs/sigmoids in each component’s functions as “linear + p RBFs.” The figures below thus compare the filtering performance of four ensemble methods: the stochastic EnKF, linear maps, and linear maps with $p \in \{1, 2\}$ RBFs.

For a fair comparison, all algorithms process the observations at a given assimilation time sequentially (see Section 3.6) and do not evaluate the likelihood function, which we assume is intractable. The stochastic EnKF computes the Kalman gain and the linear map in (3.19) by estimating the cross-covariance $\hat{\Sigma}_{\mathbf{X}, \mathbf{Y}}$ and observation variance $\hat{\Sigma}_{\mathbf{Y}}$ using data simulated from the likelihood model for each forecast sample. Since we do not require direct access to the observation operator \mathbf{H} or to the covariance of \mathcal{E}_k , these algorithms are generalizable to non-additive and non-Gaussian likelihood models. We provide examples with a nonlinear observation model and non-Gaussian observation noise in Appendices E and F, respectively.

As described in Section 3.6, the linear map algorithm is related to the stochastic EnKF. The only difference between these two algorithms lies in the way they exploit structure for the purpose of regularization. While stochastic EnKFs exploit decay of correlation between the variables with increasing spatial distance, regularization in the stochastic map filter enforces sparsity in the map $S^{\mathcal{X}}$, based on conditional independence, decay of correlation, and local likelihood structure (see Sections 3.5 and 3.6). In the stochastic map filter, the sparsity structure is parameterized by the distance r that defines the set of input state variables for each component in (3.14), and by the number of components $j \leq n$ where $S^{\mathcal{X}}$ departs from the identity map (see Remark 3). In the stochastic EnKF, covariance localization is applied by multiplying the forecast covariance elementwise with a Gaspari–Cohn tapering function that has an optimally tuned localization radius [34]. While the linear maps and the stochastic EnKF behave similarly with larger ensemble sizes—where less regularization is needed—the results may differ for small M .

All algorithms considered in this section are implemented with multiplicative prior inflation and localization. For the inflation, we increased the spread of the forecast ensemble that is used to estimate $S^{\mathcal{X}}$. We inflated these samples by multiplying their deviations from the sample mean by a scalar $\zeta \geq 1$. The parameters (i.e., inflation parameter ζ and localization parameters r and j) are tuned for each ensemble size and problem configuration to minimize the time-averaged RMSE. Only the tuned results are presented below, unless otherwise indicated. Lastly, for the $p \in \{1, 2\}$ stochastic map filter we also investigated the sensitivity of the results with respect to the scaling parameter γ of the RBFs (described in Appendix A) and found no significant dependence. Thus, the results are presented below for a fixed value of $\gamma = 2.0$ across all of the experiments.

4.2. Lorenz-63

We first consider the Lorenz-63 system without any form of localization applied to $S^{\mathcal{X}}$. The idea is to isolate the effect of adding nonlinear terms to the prior-to-posterior update. In this case, the states of the system are fully observed (i.e., $n = d$) with Gaussian observational noise and variance $\theta^2 = 4$. The time between observations is set to $\Delta t_{\text{obs}} = 0.1$. The resulting average RMSE, for a range of M , is plotted on the left of Figure 7.

For very small M , linear maps have the most robust performance. However, for sufficiently large ensemble sizes, we observe a consistent improvement in RMSE by adding nonlinearities to the approximation space of the map. Specifically, the stochastic map filter with $p = 1$ RBFs yields better tracking performance for $M \geq 40$, while the filter with $p = 2$ RBFs provides improved results for $M \geq 200$. In both cases, the improvement in average RMSE is more than 20%. The average RMSE values obtained with increasing map nonlinearity (for large enough M) also tend towards the RMSE of our “reference” solution—obtained with a consistent SIR particle filter using $M = 10^6$ samples (with an average relative effective sample size of 0.89), which we plot in Figure 7 as a dotted line.

While this experiment did not involve map localization or covariance tapering in the EnKF, the difference between the stochastic EnKF and the linear map results for small M can be attributed to the local likelihood structure that we exploit. When assimilating scalar observations $Y = y^*$ with a local likelihood model (i.e., Y only depends on one component of the state, say Z_1 after a permutation), the states Z_k for $k = 2, \dots, n$ are conditionally independent of Y given Z_1 . This Markov property results in sparsity of the KR rearrangement from $\pi_{\mathbf{X}, Y}$ to $\mathcal{N}(\mathbf{0}, \mathbf{I}_{n+1})$, and hence the map $S^{\mathcal{X}}$ (see Section 3.5). In particular, the components U^k do not depend on y for $k \geq 2$. We note that this sparsity is exact, and thus different from any approximate conditional independence that could further be exploited to regularize the estimation of $S^{\mathcal{X}}$.

In a second experiment, we investigate the performance of the stochastic map filter as a function of the time Δt_{obs} between observations, for a fixed ensemble size. The idea is to test the filter for a sequence of increasingly non-Gaussian forecast distributions. The average RMSE of the various algorithms for $\Delta t_{\text{obs}} \in [0.1, 0.5]$ and for $M = 1000$ is shown in the right panel of Figure 7. The stochastic map filters demonstrate a consistently lower RMSE over the full range of inter-observation times. This shows that map filters of increasing complexity remain stable (and continue to provide more accurate tracking) even as the state evolution becomes more nonlinear.

For this low-dimensional problem, we also investigate how the stochastic map filter captures the true filtering distribution (i.e., the sequence of posteriors $\pi_{\mathbf{X}_k | \mathbf{y}_{1:k}^*}$) over time. We first use an SIR particle filter with 10^6 samples to estimate the posterior mean \mathbf{z}_k^{PF} and posterior covariance matrix Σ_k^{PF} at each step k , with $\Delta t_{\text{obs}} = 0.1$. In Figure 8, we plot, for each algorithm, the normalized L_2 error in the posterior mean, defined as $\|\bar{\mathbf{z}}_k - \mathbf{z}_k^{\text{PF}}\|_2 / \sqrt{n}$, and the normalized error in the posterior covariance, defined as $\|\hat{\Sigma}_k - \Sigma_k^{\text{PF}}\|_F / n$, averaged over 2000 assimilation times k . We observe a significant improvement in the approximation of these posterior statistics, just by introducing a few nonlinearities in the prior-to-posterior

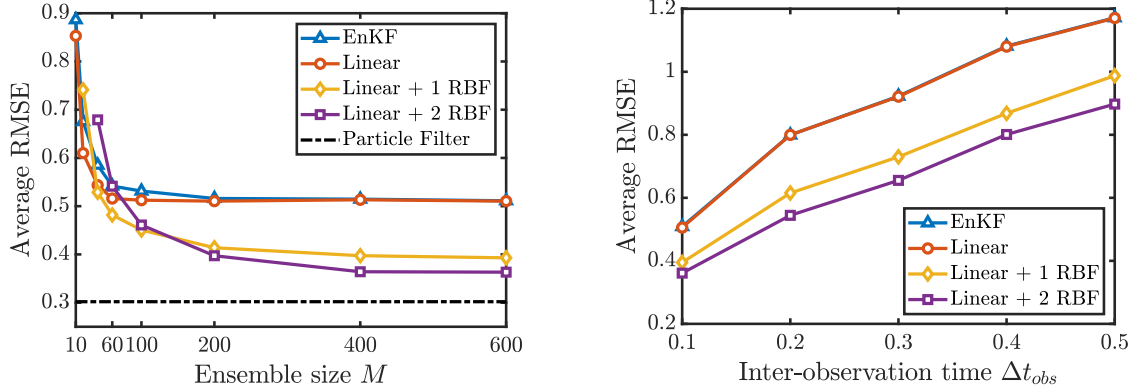


Fig 7: Average RMSE of the Lorenz-63 model for $\Delta t_{obs} = 0.1$ as a function of M (*left*), and for $M = 1000$ as a function of the inter-observation time Δt_{obs} (*right*).

transformation. For a sufficiently large M , the improvement can be more than 50%.

To characterize the variability of the particle filter estimates used above, we repeat the assimilation exercise with the reference $M = 10^6$ SIR filter for 100 times. We compute the sample standard deviations of these replicated filtering results (e.g., of the L_2 norm of the posterior mean and the Frobenius norm of the posterior covariance matrix at each assimilation time) and plot their maxima over time using dotted lines in Figure 8. For comparison, the standard errors of the same norms of posterior moments estimated with the stochastic map filter, for $M \in [20, 600]$, are 4 to 10 times smaller than the standard errors of the $M = 10^6$ SIR filter.

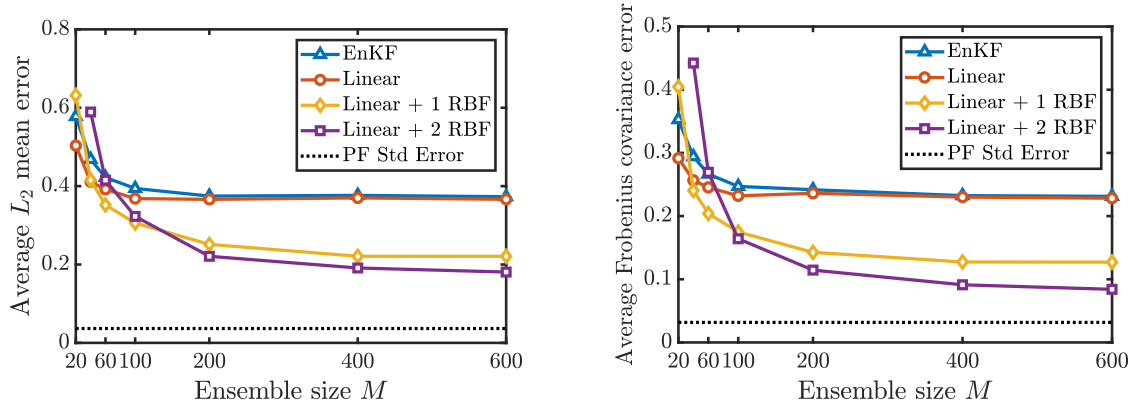


Fig 8: Normalized L_2 error of the posterior mean (*left*) and Frobenius error of the posterior covariance matrix (*right*) for the Lorenz-63 model.

4.3. Lorenz-96 with long inter-observation time

Here, we follow the “hard case” setup of [44, 7] for the Lorenz-96 model, with sparse observations in space and time, i.e., $d = 20$ (observing every other component of the state)

and $\Delta t_{\text{obs}} = 0.4$. Each observation has independent additive Gaussian noise with variance $\theta^2 = 0.5$. For reference, we note that a $\Delta t_{\text{obs}} = 0.05$ would correspond to roughly 6 hours in a global weather model [48, 49]. The large time interval between observations makes the forecast distribution highly non-Gaussian. As a result, this configuration typically requires ensemble sizes greater than the state dimension n to track \mathbf{z}_k^* . Furthermore, with a high-dimensional state vector it is necessary to tune the map’s localization parameters to achieve stable filtering performance over time. As described in Section 4.1, we tune the localization parameters r and j for the stochastic map filter and the localization radius for the EnKF, and the inflation parameter ζ for both algorithms. Figure 9 shows the sensitivity of the average RMSE for the nonlinear filters to the localization parameters. For large ensemble sizes, RMSE improves when increasing the number of non-identity map components j and the neighborhood size r . For each setting of these parameters, the filter with $p = 2$ RBFs (right) offers a slight benefit over the filter with $p = 1$ RBFs (left). We emphasize that increasing j , r , and p , for any $p \geq 1$, *all* comprise ways of increasing the nonlinearity of the map: not just via the choice of approximation space for \mathbf{u} , but also by expanding where in the map—and in which variables—nonlinearity appears.

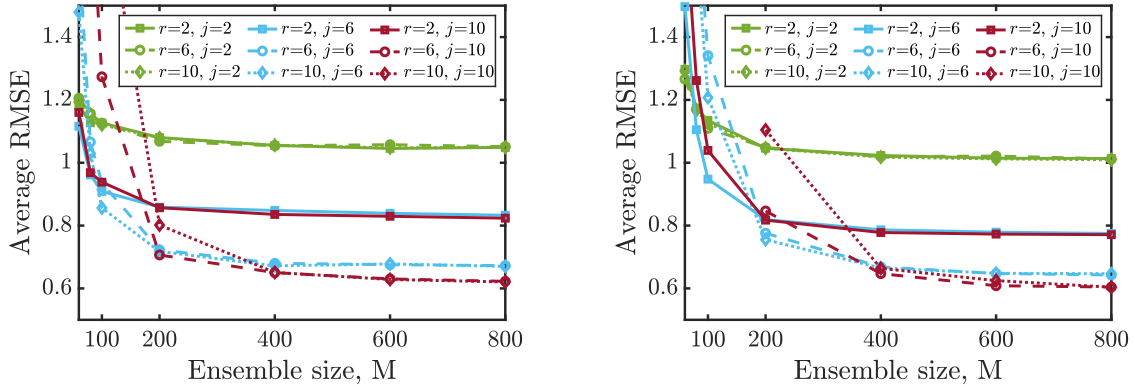


Fig 9: Average RMSE (over 2000 assimilation cycles) for the “hard” Lorenz-96 configuration of Section 4.3 using ‘linear + 1 RBF’ maps (*left*) and ‘linear + 2 RBF’ maps (*right*) for different localization parameters: the number of non-identity components j in the map $\mathcal{S}^{\mathcal{X}}$, and the neighborhood size r defining the input dependence of each map component.

Figure 10 shows the average and median values of RMSE_k (over 2000 terminal assimilation cycles k) for the optimal setting of the localization parameters as a function of the ensemble size $M \in [60, 800]$. By increasing the nonlinearity of the map $\widehat{\mathcal{S}}^{\mathcal{X}}$ and hence \widehat{T} , the stochastic map filter can reduce the bias of the EnKF given sufficient samples. For example, the plateaus of RMSE in Figure 10 for the EnKF reflect the limitation of the EnKF’s affine transformation: the RMSE initially decreases, then stagnates with increasing M . Nonlinear maps reduce the values of these plateaus (by roughly 25% in this example) and provide smaller RMSE even at intermediate ensemble sizes. By introducing relatively few nonlinear basis functions (in $\widehat{\mathcal{S}}^{\mathcal{X}}$) whose parameters can be *reliably* learned, the stochastic map filter can better capture the non-Gaussian forecast statistics and improve the tracking of \mathbf{z}_k^* .

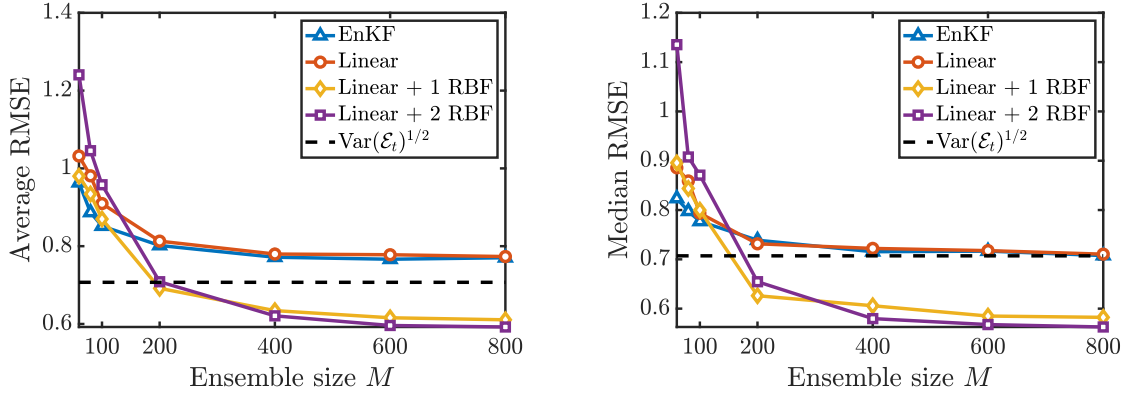


Fig 10: Average (*left*) and median (*right*) RMSE (over 2000 assimilation cycles) for the “hard” Lorenz-96 configuration of Section 4.3, with $\Delta t_{obs} = 0.4$, observing every other component of the state ($d = 20$) with additive Gaussian observational noise. Dashed line is the standard deviation of the observational noise.

Figure 10 also exposes the bias-variance tradeoff in learning the prior-to-posterior map T , which corresponds to a link between M and the complexity of the map (i.e., the number of the basis functions in each component of $S^{\mathcal{X}}$). For smaller ensemble sizes, a richer class of nonlinear maps yields estimators \hat{T} with less bias but higher variance. The EnKF and linear maps, on the other hand, yield more biased but potentially lower-variance estimators that offer more stable tracking performance for small M . In the present experiments, as M increases, the map class yielding the minimum RMSE evolves quickly from linear to $p = 1$ and then to $p = 2$. Similarly, in Figure 9, the expressiveness of the best nonlinear map class, as captured by larger localization parameters, increases with M . Overall, the stochastic map filter provides a flexible framework for adjusting the complexity of the map to the given ensemble size in order to extract a good estimator of T .

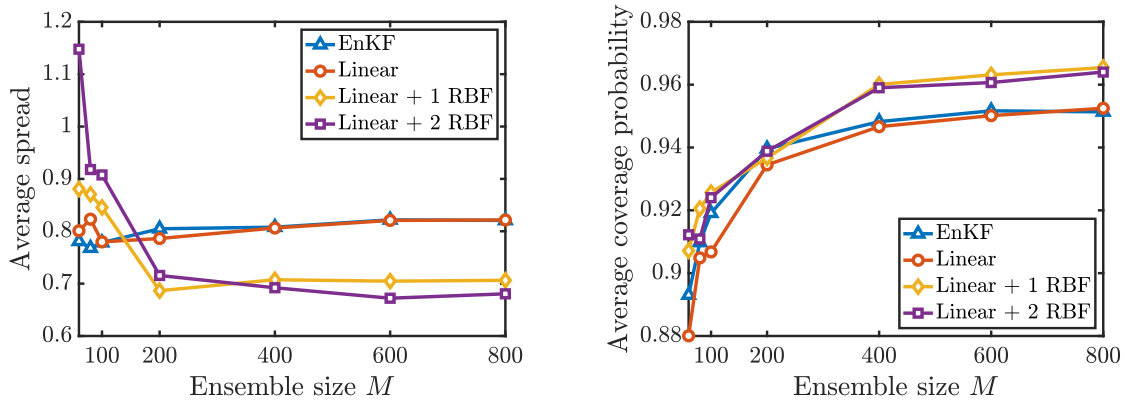


Fig 11: Average ensemble spread (*left*) and average coverage probability of the [2.5%, 97.5%] empirical intervals of each state marginal (*right*) for the “hard” Lorenz-96 configuration. (See precise definitions of these quantities in Section 4.1.)

In addition to improving the RMSE, the nonlinear stochastic map filter reduces the ensemble spread while simultaneously increasing the probability of covering the true state. We present these results for increasing M in Figure 11.

5. Discussion

We have introduced a class of nonlinear filtering algorithms based on the construction of stochastic or deterministic couplings between continuous distributions. These algorithms generalize the EnKF to nonlinear updates of tunable *and* arbitrary complexity. The key computational task in applying these algorithms is the numerical estimation of a KR rearrangement via convex optimization. Our goal in using nonlinear updates is to reduce the intrinsic bias of the EnKF, while retaining its robustness in high dimensions. We run our numerical experiments on various configurations of the Lorenz-96 model, which is a common testbed for numerical weather prediction systems; we also include a comparison with the true (Bayesian) filtering distributions for the lower-dimensional Lorenz-63 model. Through these experiments, we show how filtering with nonlinear updates can significantly outperform the EnKF in a range of highly non-Gaussian settings, for a marginal increase in ensemble requirements and computational effort. In what follows, we briefly discuss limitations and possible extensions of this approach to filtering.

Nonlinear parameterizations Highly nonlinear updates do not automatically guarantee better filtering performance. Trying to estimate complex transformations from very few samples could yield unacceptable variance. The bias and variance of a transport map estimator must be balanced, possibly by introducing additional information through regularization. In this paper, we consider several regularization techniques. For instance, we define a hierarchy of nonlinear (separable) parameterizations for the transport maps that allow for a gradual departure from the linear *ansatz*, which is key to reducing the bias while managing the variance of the estimator. We select the “best” parameterization according to a prediction error criterion. We notice several intuitive trends. Increasingly nonlinear transformations typically demand larger ensembles, while for a fixed parameterization of the maps, the tracking error plateaus beyond a certain ensemble size. Similarly, for any given problem, we expect there to be a sufficiently small ensemble size for which the linear *ansatz*—as in EnKF techniques—performs best. Moreover, for nonlinear filtering problems that are well approximated by Gaussian distributions, we do not expect major gains from using nonlinear updates, even for large ensemble sizes. Nonlinear updates are mostly needed to capture non-Gaussian structure. The complexity of the transformations should then be adapted to the number of ensemble members and to the non-Gaussianity of the problem. Certainly many avenues exist for increasing this complexity. Here we focused on separable parameterizations, motivated in part by computational simplicity, but much more so by the fine-grained control over complexity that they enable. General non-separable maps could be considered as well; see [6] for a recent contribution in this direction. In future work, we wish to automate this adaptation rather than running an offline calibration phase, i.e., we plan to develop *nonparametric* extensions of the proposed filtering algorithms. For any

of these choices, we emphasize that the estimate of the resulting *composed* transformation T —and its expressivity in acting on the forecast distribution—is what ultimately affects the filtering approximation.

Localization and other form of regularization A related regularization idea is that of exploiting decay of correlation and approximate conditional independence in the filtering distribution. This structure is common when filtering spatiotemporal processes. In this paper, we introduced simple *localization* ideas for nonlinear updates by imposing specific sparsity patterns in the transport maps composing the update. In future work, one could explore a much wider range of regularization techniques. For instance, it is natural to consider LASSO-type estimators in order to “discover”—rather than to enforce—sparsity of the nonlinear transformations. Or one might exploit low-rank structure in the change from forecast to filtering distribution in order to reduce the effective dimension of the nonlinear update, following the line of work in [72, 19]. Accounts of low-rank structure in transport maps can be found in [70, Ch. 5] and [13]; for an initial application to filtering, see [43]. In general, we believe that practical high-dimensional filtering relies crucially on the development of structure-exploiting regularization techniques.

Consistency From a theoretical point of view, it would be interesting to study the behavior of the proposed algorithms in a simultaneous limit of increasing ensemble size *and* increasing complexity of the rearrangements. In particular, a key goal should be to understand conditions under which it is possible to establish some form of *consistency* for the filters, much in the same spirit as the convergence theory for SMC methods [18]. This question is meaningless for the EnKF, which is inherently inconsistent due to the fixed linear structure of the update. It would also be interesting to understand the stochastic map filter in a continuous-time filtering setting, and thus to explore its connections with the feedback particle filter [80]. This link might offer further insight into conditions that ensure consistency.

Further extensions The ideas presented in this paper can readily be extended to *smoothing*, i.e., characterizing the conditional distribution of past states, given all available measurements. In this context, one can first estimate a (non-singular) Markov transition kernel between observation times via an upper-triangular KR rearrangement, and then use this approximation to propagate the filtering ensemble backwards in time. The resulting scheme can be interpreted as a Monte Carlo approximation of the transport map backward-smoothing algorithm introduced in [71, Section 7]. It would then be interesting to explore connections with the multi-level generalizations presented in [33]. Relatedly, it would be useful to extend the present framework to problems of sequential *joint parameter and state* estimation.

Finally, we note that the analysis step of the stochastic map filter is an instance of *approximate Bayesian computation*, as it requires only sampling from the likelihood and prior in order to construct a prior-to-posterior transformation. Realizing and expanding

this approach for generic problems of simulation-based inference [17] represents an exciting avenue for future work.

Acknowledgments

AS, RSB, and YMM gratefully acknowledge support from the AFOSR Computational Mathematics program and AFOSR MURI award FA9550-15-1-0038, and from the US Department of Energy, Office of Advanced Scientific Computing Research, AEOLUS project. RSB also acknowledges support from an NSERC PGSD-D Fellowship. AS acknowledges support from the Deutsche Forschungsgemeinschaft (DFG), through the CRC 1294 “Data Assimilation” Project, for a visit to the Institute for Mathematics of the University of Potsdam. The authors also thank Daniele Bigoni, Jana de Wiljes, Matthias Morzfeld, Sebastian Reich, and Xin Tong for many insightful discussions and suggestions.

Appendix A: Parameterization and computation of monotone triangular maps

In this section, we first discuss possible parameterizations for a monotone triangular map U that is meant to approximate the KR rearrangement between a pair of densities on \mathbb{R}^n (Section 3.4). Then, we link specific structures in the parameterization of U to computational simplifications for an estimator of the rearrangement.

The KR rearrangement between a pair of positive densities is a triangular bijection on \mathbb{R}^n such that each slice (3.3) is strictly increasing and absolutely continuous [11]. Hence, it makes sense to consider candidate rearrangements U whose k th components, U^k , can be written as

$$U^k(z_1, \dots, z_k) = a_k(z_1, \dots, z_{k-1}) + \int_0^{z_k} \exp(b_k(z_1, \dots, z_{k-1}, t)) dt, \quad (\text{A.1})$$

for some *arbitrary* functions (a_k, b_k) , and for all $k = 1, \dots, n$ [62, 52]. For any choice of (a_k, b_k) , the rearrangement U is a strictly monotone (increasing) triangular map, since $\partial_k U^k = \exp(b_k) > 0$ for all k . In fact, (A.1) provides a rather general way to represent monotone triangular functions.

The estimator in (3.10) relies on the definition of an approximation space, \mathcal{H}_k , for every component of the rearrangement. A viable strategy is to use the monotone representation in (A.1) and to constrain each function (a_k, b_k) to lie in a finite dimensional space, i.e.,

$$a_k(\mathbf{z}) = \sum_i a_i \psi_i^a(\mathbf{z}), \quad b_k(\mathbf{z}) = \sum_j b_j \psi_j^b(\mathbf{z}), \quad (\text{A.2})$$

for a collection of finitely many basis functions ψ_i^a, ψ_j^b —e.g., multivariate Hermite polynomials, Hermite functions, splines, or radial basis functions—and unknown real valued coefficients (a_i, b_j) .¹⁰ The minimization in (3.10) can then be cast in terms of the unknown coefficients, which fully parameterize the maps in \mathcal{H}_k .

¹⁰We may substitute the exponential in (A.1) with a square function or even a sum of squares [35]. This offers the computational advantage of precomputing any integral in (A.1) once and for all, thanks to parameterizations of b_k that are linear in the unknown coefficients (see [10]).

As explained in Section 3.5, the “complexity” of each \mathcal{H}_k is a key ingredient for regularizing the estimation of the rearrangement; there is no point in trying to learn arbitrarily nonlinear maps from a given finite ensemble. For instance, the EnKF restricts the search to linear maps. In general, it is possible to depart from the linear ansatz in a *gradual* way, by imposing structural assumptions of increasing complexity on the rearrangement. For example, we can consider maps whose components are separable as sums of *univariate* nonlinear functions (\mathbf{u}_i) that each admit a linear parameterization like (A.2) or (A.1) (if monotone), i.e.,

$$U^k(z_1, \dots, z_k) = \mathbf{u}_1(z_1) + \dots + \mathbf{u}_k(z_k). \quad (\text{A.3})$$

Next, we can consider separable parameterizations in terms of bivariate functions, i.e., $U^k(z_1, \dots, z_k) = \sum_{i \leq k} \mathbf{u}_i(z_i, z_k)$, and so on. In essence, the complexity of the parameterization should be adapted (and calibrated) to the cardinality of the ensemble and to the amount of prior information that is injected in the estimation (e.g., see the localization ideas of Section 3.4).

In the numerical examples of this paper, we explore the separable parameterization in (A.3), since we wish to work with ensemble sizes comparable to those needed by the EnKF. We propose a specific strategy to parameterize each \mathbf{u}_i in (A.3), although there are plenty of potential alternatives. For $i < k$, \mathbf{u}_i is simply a univariate function, not necessarily monotone. In this case, we parameterize \mathbf{u}_i as a linear combination of p radial basis functions (RBFs) plus a global linear term, i.e.,

$$\mathbf{u}_i(z) = u_{i0} z + \sum_{j=1}^p u_{ij} \mathcal{N}(z; \xi_j, \sigma_j^2), \quad (\text{A.4})$$

for a collection of centers $\boldsymbol{\xi} := (\xi_1, \dots, \xi_p)$, scale parameters $\boldsymbol{\sigma} := (\sigma_1, \dots, \sigma_p)$, and unknown coefficients (u_{ij}). The number p of RBFs defines the degree of nonlinearity of \mathbf{u}_i . For $p = 0$, \mathbf{u}_i reverts to a linear function. The centers $\boldsymbol{\xi}$ are chosen from p (uniform) empirical quantiles of the marginal distribution of the ensemble along the i th coordinate direction, i.e., $\xi_j := \hat{q}_{j/(p+1)}$ for $j = 1, \dots, p$, where for any $\alpha \in (0, 1)$, \hat{q}_α denotes the α -th empirical quantile. The scale parameters $\boldsymbol{\sigma}$ are defined to be proportional to the inter-distance between the centers $\boldsymbol{\xi}$, i.e., $\sigma_j := \gamma (\xi_{j+1} - \xi_{j-1})/2$ for $j = 1, \dots, p$, where $\xi_0 := \xi_1$, $\xi_{p+1} := \xi_p$, and where $\gamma > 0$ is a tuning parameter. In our experiments, we consider $\gamma \in [1, 3]$. The parameterization of \mathbf{u}_k in (A.3) is a bit different, since the monotonicity constraint on U^k requires \mathbf{u}_k to be an increasing map. One option is to use the monotone representation in (A.1) just for \mathbf{u}_k . In practice, however, \mathbf{u}_k is a univariate function and thus we can seek alternative ways of imposing monotonicity, e.g., by expressing \mathbf{u}_k as a nonnegative combination of monotone basis functions. For a monotone \mathbf{u}_k , its derivative $\partial \mathbf{u}_k$ is always nonnegative. For $p > 0$, we propose to parameterize $\partial \mathbf{u}_k$ with $p + 2$ positive basis functions, i.e., $\partial \mathbf{u}_k = \sum_{j=0}^{p+1} u_{kj} \psi'_j$, where $\psi'_j(z) := \mathcal{N}(z; \xi_j, \sigma_j^2)$ for $j = 1, \dots, p$, while

$$\psi'_0(z) := \frac{1}{2} - \frac{1}{2} \operatorname{erf} \left(\frac{z - \xi_0}{\sqrt{2} \sigma_0} \right), \quad \text{and} \quad \psi'_{p+1}(z) := \frac{1}{2} + \frac{1}{2} \operatorname{erf} \left(\frac{z - \xi_{p+1}}{\sqrt{2} \sigma_{p+1}} \right), \quad (\text{A.5})$$

for a collection of $p + 2$ centers (ξ_i) and scale parameters (σ_i). The centers and scale parameters are chosen similarly to those in (A.4), i.e., from uniform empirical quantiles of the marginal distribution of the ensemble along the k th direction. Intuitively, $\partial \mathbf{u}_k$ is the linear combination of p RBFs (ψ'_1, \dots, ψ'_p) plus a pair of positive functions (ψ'_0, ψ'_{p+1}) that revert to constants in the tails. The idea is to promote robustness by constraining \mathbf{u}_k to be linear in the tails. Non-negativity of $\partial \mathbf{u}_k$ is imposed by the set of linear inequalities $u_{kj} \geq 0$, for $j = 0, \dots, p + 1$. The resulting monotone parameterization of \mathbf{u}_k is obtained by integrating $\partial \mathbf{u}_k$, i.e., $\mathbf{u}_k(z) := \int_0^z \partial \mathbf{u}_k(x) dx = c + \sum_{j=0}^{p+1} u_{kj} \psi_j(z)$, for an unknown constant c and antiderivatives $\psi_j := \int \psi'_j$ given by

$$\begin{cases} \psi_0(z) = \frac{1}{2} \left((z - \xi_0) (1 - \operatorname{erf}(\Delta_0)) - \sigma_0 \sqrt{2/\pi} \exp(-\Delta_0^2) \right) \\ \psi_j(z) = \frac{1}{2} (1 + \operatorname{erf}(\Delta_j)) & \text{for } 1 \leq j \leq p \\ \psi_{p+1}(z) = \frac{1}{2} \left((z - \xi_{p+1}) (1 + \operatorname{erf}(\Delta_{p+1})) + \sigma_{p+1} \sqrt{2/\pi} \exp(-\Delta_{p+1}^2) \right) \end{cases} \quad (\text{A.6})$$

where $\Delta_j := (z - \xi_j)/(\sqrt{2}\sigma_j)$ for all j . For $p = 0$, we set \mathbf{u}_k to be an affine function. For the parameterization of U^k given by (A.4) and (A.6), the minimization in (3.10) is a linearly constrained convex program that can be solved efficiently via numerical optimization, e.g., using the projected Newton's method [8]. Moreover, if \mathbf{u}_k is parameterized by an affine function, then (3.10) reduces to a standard *linear regression* problem with a closed form solution. We analyze this fact in the more general case of parameterizations that are separable *only* in the last (monotone) variable, i.e.,

$$U^k(z_1, \dots, z_k) = \mathbf{u}(z_1, \dots, z_{k-1}) + \mathbf{u}_k(z_k), \quad (\text{A.7})$$

where $\mathbf{u}(z) = \sum_j u_j \psi_j(z)$ for a collection of arbitrary basis functions (ψ_j) and where $\mathbf{u}_k(z) = c + \alpha z$. In this case, we can rewrite (3.10) as

$$\min_{(\tilde{u}_j, \tilde{c}, \alpha} \frac{\alpha^2}{2} \left\{ \frac{1}{M} \sum_{i=1}^M \left(\sum_j \tilde{u}_j \psi_j(z_1^i, \dots, z_{k-1}^i) + \tilde{c} + z_k^i \right)^2 \right\} - \log \alpha, \quad (\text{A.8})$$

where $\mathbf{z}^i = (z_1^i, \dots, z_n^i)$, $\tilde{c} := c/\alpha$, and $\tilde{u}_j := u_j/\alpha$ for all j . The minimization of (A.8) with respect to the new variables (\tilde{c}, \tilde{u}_j) can be done independently of α , and corresponds to a standard regression problem, i.e.,

$$\kappa^* := \min_{(\tilde{u}_j, \tilde{c})} \frac{1}{M} \sum_{i=1}^M \left(\sum_j \tilde{u}_j \psi_j(z_1^i, \dots, z_{k-1}^i) + \tilde{c} + z_k^i \right)^2, \quad (\text{A.9})$$

while the optimal α is given by $1/\sqrt{\kappa^*}$.

Appendix B: Deterministic map filter with conditionally independent and local observations

In many problems of interest, we have conditionally independent and local observations, i.e.,

$$\pi_{\mathbf{Y}|\mathbf{X}} = \prod_{k=1}^d \pi_{Y_k|X_{\ell_k}}, \quad (\text{B.1})$$

for a subset of d state variables (X_{ℓ_k})—possibly up to a whitening transformation of the state [34, 53]. In Section 3.6, we saw that (B.1) implies that we can process each of the d scalar observations individually and sequentially. For the deterministic map filter, there is a strong incentive in processing scalar observations one at a time, because we can avoid the explicit solution of a non-convex problem like (3.25).

Without loss of generality, let us assimilate a scalar observation, y^* , of the *first* state variable, possibly up to a permutation. The corresponding likelihood function is given by $\pi_{Y|X_1}$. We want to define a structure-exploiting analysis map T , similar to (3.22). Let S be a KR rearrangement that pushes forward $\pi_{\mathbf{X}}$ to a standard normal $\eta := \mathcal{N}(\mathbf{0}, \mathbf{I}_n)$ —as in (3.22)—and let $\eta_1 := \mathcal{N}(0, 1)$ denote the marginal of η along the first variable. By the definition of KR rearrangement, the pullback of η_1 by the first component, S^1 , of S is equivalent to the prior marginal along the observed component, i.e., $(S^1)^\# \eta_1 = \pi_{X_1}$. Moreover, for all univariate monotone maps \mathbf{u} , define $\pi_{\mathbf{u}}$ to be the density that is proportional to the function $\xi \mapsto \pi_{Y|X_1}(y^*|\xi) \mathbf{u}^\# \eta_1(\xi)$, which is the product of likelihood and pullback $\mathbf{u}^\# \eta_1$. Note that π_{S^1} is equivalent to the posterior marginal $\pi_{X_1|y^*}$. Let \mathbf{m} be the increasing rearrangement on \mathbb{R} —really a one-dimensional KR rearrangement—that pushes forward η_1 to π_{S^1} , and notice that the posterior distribution factorizes as

$$\pi_{\mathbf{X}|y^*} = \pi_{X_1|y^*} \pi_{\mathbf{X}_{2:n}|X_1}, \quad (\text{B.2})$$

because of the local structure of the likelihood function. The map \mathbf{m} characterizes the posterior marginal $\pi_{X_1|y^*}$, while S gives access to the prior conditional $\pi_{\mathbf{X}_{2:n}|X_1}$. To see this, notice that for all $z \in \mathbb{R}$, the map

$$z_2, \dots, z_n \mapsto \begin{bmatrix} S^2(z, z_2) \\ \vdots \\ S^n(z, z_2, \dots, z_n) \end{bmatrix} \quad (\text{B.3})$$

pushes forward the conditional $\pi_{\mathbf{X}_{2:n}|X_1}(\cdot|z)$ to a standard normal on \mathbb{R}^{n-1} (cf. Section 3.2). Hence, we can define the analysis map T as follows,

$$T := S_{\mathbf{Id}}^{-1} \circ \mathcal{M} \circ S, \quad (\text{B.4})$$

where $S_{\mathbf{Id}}$ coincides with S except for the first component, which is set to the identity

function,

$$S_{\mathbf{Id}}(\mathbf{z}) := \begin{bmatrix} z_1 \\ S^2(z_1, z_2) \\ \vdots \\ S^n(z_1, z_2, \dots, z_n), \end{bmatrix}, \quad \text{and} \quad \mathcal{M}(\mathbf{z}) := \begin{bmatrix} \mathbf{m}(z_1) \\ z_2 \\ \vdots \\ z_n \end{bmatrix}. \quad (\text{B.5})$$

It is immediate to verify that T pushes forward $\pi_{\mathbf{X}}$ to $\pi_{\mathbf{X}|y^*}$. In particular, the map \mathcal{M} is responsible for incorporating information from the measurement y^* only in the observed component of the state—this is a *local assimilation* step—while the map $S_{\mathbf{Id}}^{-1}$ is responsible for *propagating information* to the remaining components. In practice, we just showed that, when assimilating a local scalar observation, the map \mathcal{T} in (3.22) can be rewritten as $\mathcal{T} = S_{\mathbf{Id}}^{-1} \circ \mathcal{M}$.

We propose to estimate T by \widehat{T} ,

$$\widehat{T} := \widehat{S}_{\mathbf{Id}}^{-1} \circ \widehat{\mathcal{M}} \circ \widehat{S}, \quad (\text{B.6})$$

where \widehat{S} is the usual maximum likelihood estimator of the KR rearrangement S (Section 3.4), $\widehat{S}_{\mathbf{Id}}$ is an estimator of $S_{\mathbf{Id}}$ obtained (for free) by selecting the corresponding components of \widehat{S} , while $\widehat{\mathcal{M}}$ is defined by an estimator, $\widehat{\mathbf{m}}$, of the increasing rearrangement \mathbf{m} that pushes forward a standard normal to $\pi_{\widehat{S}_1}$. The latter is an approximation of the posterior marginal, $\pi_{X_1|y^*}$, which depends only on the first component of \widehat{S} .

In principle, we could define $\widehat{\mathbf{m}}$ to be the solution of a non-convex minimization problem like (3.25), for some parameterization of the rearrangement, which is now just a one dimensional function, and thus easier to represent than a general rearrangement on \mathbb{R}^n . In practice, however, we can simply target a different characterization of the increasing rearrangement in terms of CDFs. If $F : \mathbb{R} \rightarrow [0, 1]$ is the CDF of $\mathcal{N}(0, 1)$ and $F_{\pi_{\widehat{S}_1}} : \mathbb{R} \rightarrow [0, 1]$ is the CDF of $\pi_{\widehat{S}_1}$, then we can express \mathbf{m} as

$$\mathbf{m} = F_{\pi_{\widehat{S}_1}}^{-1} \circ F, \quad (\text{B.7})$$

and thus $\widehat{\mathbf{m}}$ can be any estimator of (B.7). There are many options here, from parametric to fully nonparametric estimators. We propose the following strategy. For a collection of N grid points (x_1, \dots, x_N) on \mathbb{R} , let f_i denote an approximation of $F_{\pi_{\widehat{S}_1}}(x_i)$ obtained via numerical integration (recall that we can evaluate the density $\pi_{\widehat{S}_1}$ everywhere up to a normalizing constant). Notice that $\mathbf{m}^{-1} = F^{-1} \circ F_{\pi_{\widehat{S}_1}}$ and let $\xi_i := F^{-1}(f_i)$ for all $i = 1, \dots, N$. We can think of ξ_i as an approximation of $\mathbf{m}^{-1}(x_i)$. Hence, the pairs $(\xi_i, x_i)_{i=1}^N$ yield approximate input-output evaluations of the rearrangement \mathbf{m} , and can be used to define a *convex* regression problem for the estimator $\widehat{\mathbf{m}}$,

$$\widehat{\mathbf{m}} \in \arg \min_{\mathbf{u} \in \mathcal{H}} \frac{1}{N} \sum_{i=1}^N (\mathbf{u}(\xi_i) - x_i)^2, \quad (\text{B.8})$$

for some space \mathcal{H} of univariate monotone maps (Appendix A).

We can further use localization ideas from Section 3.4 and Remark 3 to regularize the estimation of T in high dimensions.

Remark 7 (Connection with the multivariate rank histogram filter). *Intuitively, the multivariate rank histogram filter implements a nonparametric estimator of a deterministic update similar to (B.4), exploiting the factorization (B.2) of the posterior density. The idea is to (1) apply Bayes’ rule locally—along the observed component—combining the histogram approximation of π_{X_1} suggested by [4] with the likelihood function $\pi_{Y|X_1}$ to yield a piecewise constant approximation of the posterior marginal $\pi_{X_1|y^*}$, and (2) propagate information to the unobserved components by computing a sequence of (nonparametric) particle approximations of the conditionals $\pi_{X_k|\mathbf{X}_{1:k-1}}$, for $k \geq 2$. Recall that the conditionals $\pi_{X_k|\mathbf{X}_{1:k-1}}$ fully characterize the KR rearrangement S in (B.4). In high dimensions, it is increasingly challenging to deploy particle approximations of the conditionals $\pi_{X_k|\mathbf{X}_{1:k-1}}$, and thus [53] resorts to a mean-field approximation of the posterior density,*

$$\pi_{\mathbf{X}|y^*} \approx \pi_{X_1|y^*} \prod_{k=2}^n \pi_{X_k|X_1}, \quad (\text{B.9})$$

which relies only on the characterization of bivariate conditionals.

Appendix C: Continuous ranked probability score evaluations

To assess the predictive performance of our ensembles, we compute the continuous ranked probability score (CRPS) [14, 28]. The CRPS for the i th marginal component of the state at step k compares the ensemble’s empirical CDF $\hat{F}_{k,i}(z)$ with a Heaviside function centered at the true state, $H(z - (\mathbf{z}_k^*)_i)$, as given by $\text{CRPS}_{k,i} = \int (\hat{F}_{k,i}(z) - \mathbb{1}((\mathbf{z}_k^*)_i \leq z))^2 dz$. We average $\text{CRPS}_{k,i}$ over state components i and assimilation steps k .

For the Lorenz-63 model in Section 4.2, we compute the CRPS and report the average, over all three state components and 2000 assimilation cycles, for increasing M in Figure 12 (left). For $M \geq 60$ samples, the nonlinear stochastic map filter yields lower values of CRPS, which provides a simultaneous diagnostic of calibration and sharpness as defined in [28]. With increasing nonlinearity in the prior-to-posterior transformation, the average CRPS for the Lorenz-63 model approaches that of a particle filter using 10^6 samples.

For the Lorenz-96 configuration in Section 4.3 we compute the average CRPS (over the $n = 40$ state components and 2000 assimilation cycles) and report the results in Figure 12 (right). With $M \geq 100$ samples, the nonlinear stochastic map filter yields a lower CRPS than its linear counterparts. Adding more nonlinearity to the transformation allows the score to improve even further with increasing M .

Appendix D: Effect of time discretization

In this section, we repeat the Lorenz-96 filtering experiment of Section 4.3, but use a smaller stepsize $\Delta t = 0.001$ when performing numerical integration of (4.2) to generate the sequence of true hidden states and the synthetic observations $(\mathbf{y}_k^*)_k$. We maintain the larger stepsize $\Delta t = 0.01$ for numerical integration within each forecast step, prior to assimilating

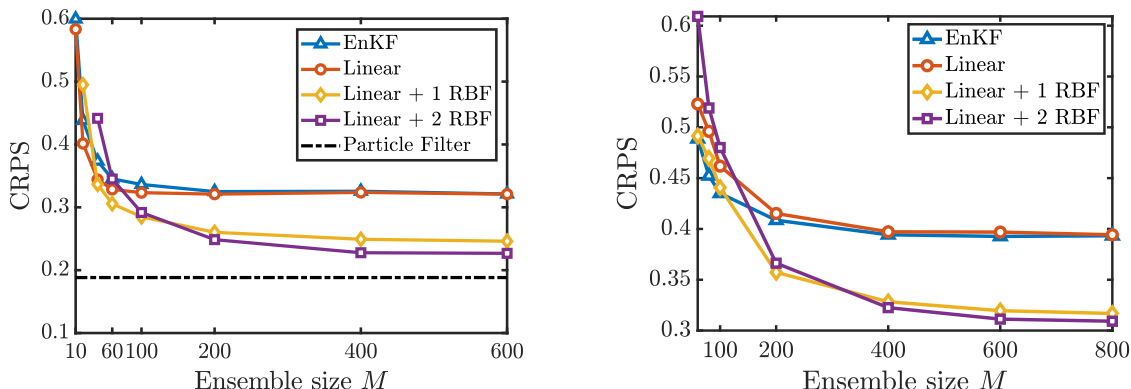


Fig 12: Average continuous rank probability score (CRPS) of the analysis ensemble for our Lorenz-63 experiments (*left*) and the “hard” Lorenz-96 configuration (*right*).

data. This mismatch ensures that there is no “inverse crime” [36] wherein the same model is used to synthesize and to invert the data. Figure 13 plots the average and median RMSE over 2000 assimilation cycles for different ensemble sizes and map parameterizations. This figure matches the trends in Figure 10, which used identical twin experiments (i.e., the same stepsize $\Delta t = 0.01$ both to generate the observations and to run the filtering algorithms). Figure 14 plots the average spread and marginal coverage probabilities of the ensemble; again, it closely follows the trends in Figure 11. We believe this insensitivity is in part due to the underlying chaotic dynamics of (4.2), as well as the noise in the observations; both prevent the model from recovering the true state exactly. Chaotic dynamics, in particular, may prevent any spurious reduction in error that might otherwise come from using common step sizes. For the filtering problems in Sections 4.2, E, and F we thus expect a similar insensitivity to the time discretization used to generate the observations, and we omit these comparisons for brevity.

Appendix E: Numerical results for Lorenz-96 model with heavy-tailed observational noise

A second challenging configuration of the Lorenz-96 model is obtained with sparse and *heavy-tailed* observations. In this setting, we consider $\Delta t_{\text{obs}} = 0.1$ and $d = 10$ (observing every fourth component of the state), and additive independent Laplace (i.e., double-exponential)-distributed observational noise. The noise has variance $2\theta^2$, where $\theta = 1$ is the scale parameter of the Laplace distribution. The large variance of the noise and limited number of observations make filtering difficult; for instance, large RMSE values are obtained when using the EnKF with ensemble sizes smaller than $M = 100$.

Similar to the results in Section 4.3, we observe improved tracking performance with increasing nonlinearity in the map $S^{\mathcal{X}}$, provided M is not too small. Figure 15 shows the average and median RMSE for the EnKF and different stochastic map parameterizations. As M increases, the bias-variance tradeoff shifts in favor of more complex maps. Furthermore,

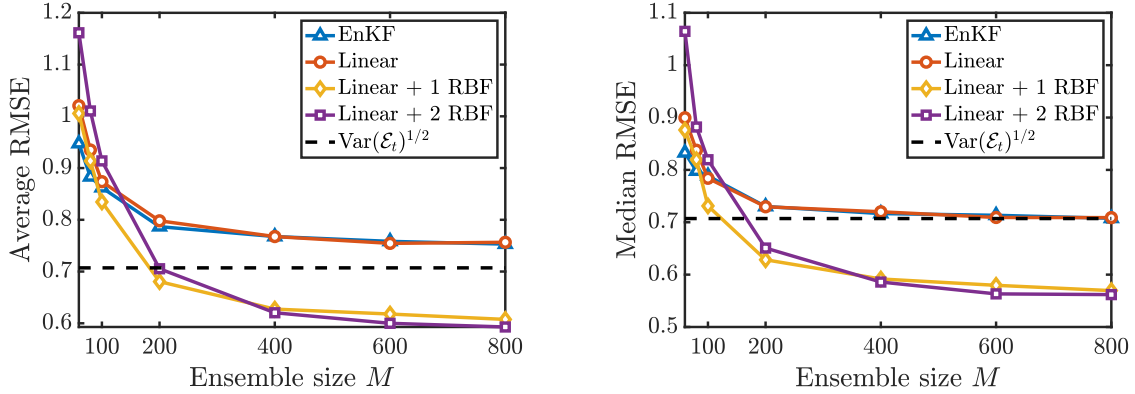


Fig 13: Average (*left*) and median (*right*) RMSE (over 2000 assimilation cycles) for the “hard” Lorenz-96 configuration. Problem setup is identical to Section 4.3, except that we use a finer numerical discretization ($\Delta t = 0.001$) to generate the observations.

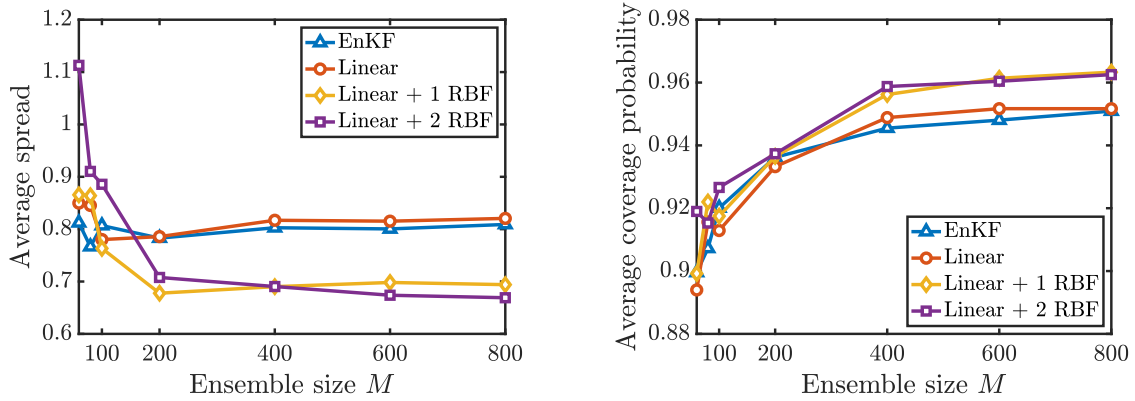


Fig 14: Average spread (*left*) and marginal coverage probabilities (*right*) (over 2000 assimilation cycles) for the “hard” Lorenz-96 configuration. Problem setup is identical to Section 4.3, except that we use a finer numerical discretization ($\Delta t = 0.001$) to generate the observations.

as illustrated in Figure 16, higher order maps also increase the average coverage probability of the ensemble across 2000 assimilation steps without increasing the ensemble spread. These results suggest that, by increasing the complexity of the prior-to-posterior transformation, ensemble members from the stochastic map filter better represent the true state \mathbf{z}_k^* and its uncertainty for problems with non-Gaussian forecast and analysis distributions.

Appendix F: Numerical results for Lorenz-96 model with nonlinear observations

In this experiment, we evaluate the applicability of the stochastic map filter to more general

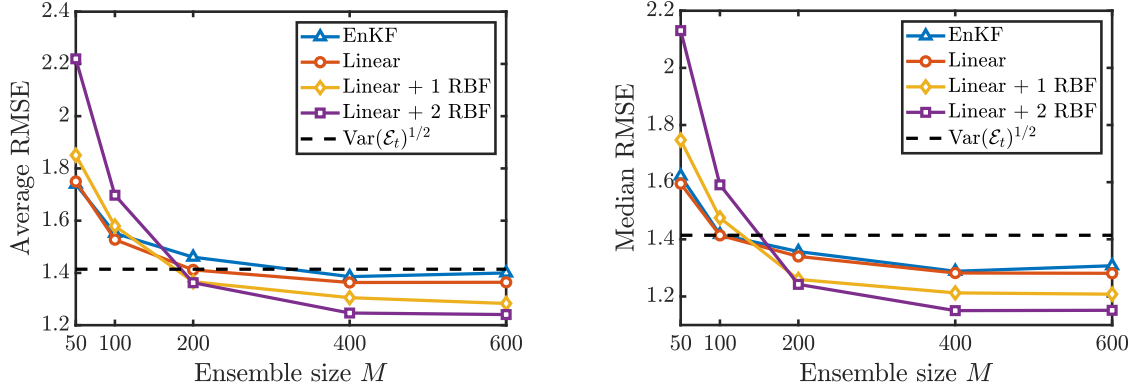


Fig 15: Average (*left*) and median (*right*) RMSE (over 2000 assimilation cycles) for the heavy-tailed (Laplace observational noise) Lorenz-96 configuration of Section E, with $\Delta t_{\text{obs}} = 0.1$ and $d = 10$ observations. Dashed line is the standard deviation of the observational noise.

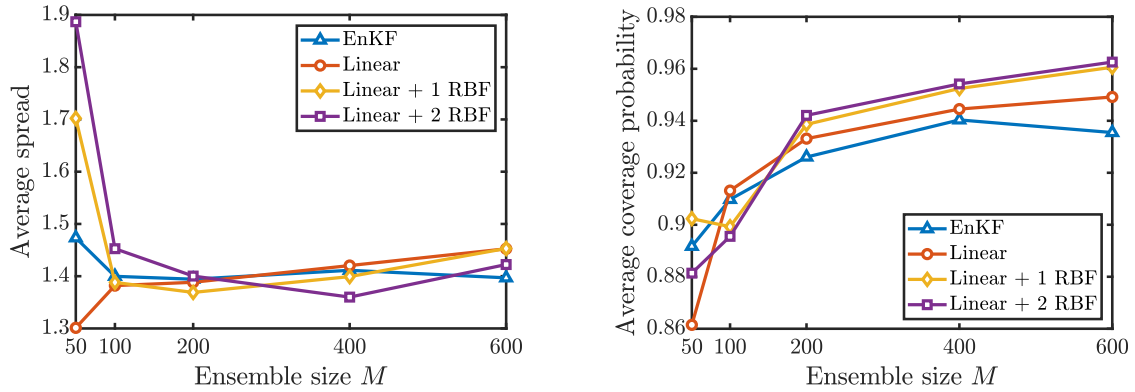


Fig 16: Average ensemble spread (*left*) and average coverage probability of the [2.5%, 97.5%] empirical intervals of each state marginal (*right*) for the heavy-tailed Lorenz-96 configuration.

likelihood models by filtering the Lorenz-96 system with *nonlinear observations* of the state. We begin with the “hard case” configuration of the Lorenz-96 system in Section 4.3, with $\Delta t_{\text{obs}} = 0.4$ (long time between observations) and $d = 20$ observations at each assimilation step (observing every other component of the state). But we modify the observation model: now each component of $\mathbf{Y}_k \in \mathbb{R}^d$ results from a nonlinear square root transformation of the corresponding state component, perturbed by additive Gaussian noise. In other words, letting $\{Y_{k,i}\}_{i=1}^d$ denote the components of \mathbf{Y}_k , we let each $Y_{k,i} = \text{sign}(Z_{k,2i-1})\sqrt{|Z_{k,2i-1}|} + \mathcal{E}_{k,i}$, where $\{\mathcal{E}_{k,i}\}_{i=1}^d \stackrel{\text{iid}}{\sim} \mathcal{N}(0, \theta^2)$ are independent of \mathbf{Z}_k . To maintain a similar signal-to-noise ratio as in the direct observation case, we use an observational noise variance of

$\theta^2 = 0.25$. A similar observation model was also studied in [5]. In this experiment, we use the map parameterization described in Section 4.1, with component functions U^k that depend linearly on the state variable z_k and nonlinearly on the other variables, for all k .

Figure 17 plots the average and median RMSE for the stochastic EnKF and stochastic map filters, over 2000 assimilation cycles. Similar to the results in Section 4.3, the stochastic EnKF and linear maps yield the lowest average RMSE at small ensemble size M , but their performance plateaus with increasing M . Nonlinear maps yield even lower RMSE for progressively larger ensemble sizes. These trends reflect the same bias-variance tradeoff as in our previous examples. Figure 18 shows that the marginal coverage probability increases monotonically with increasing map complexity, though at the same time more complex maps generally achieve smaller ensemble spread.

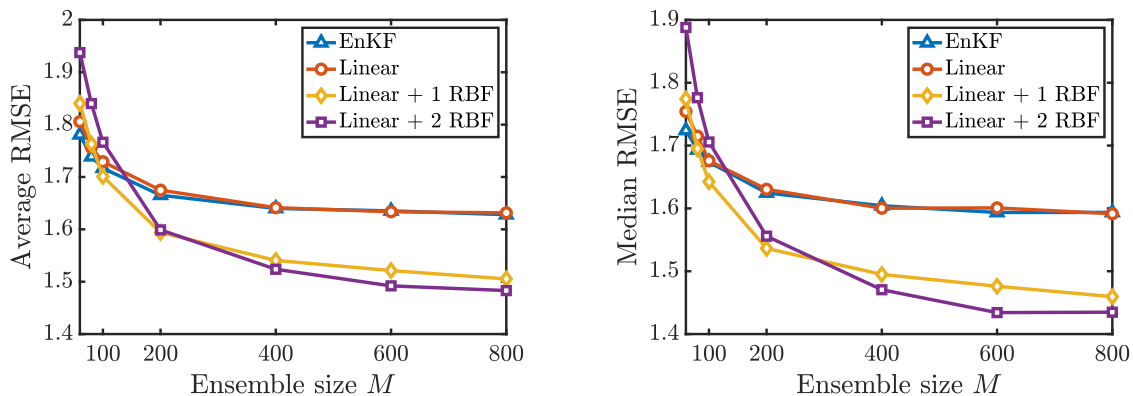


Fig 17: Average (left) and median (right) RMSE (over 2000 assimilation cycles) for the Lorenz-96 configuration of Section 4.3, with long inter-observation times, modified to have $d = 20$ square-root observations of the state.

References

- [1] ACEVEDO, W., DE WILJES, J. and REICH, S. (2017). Second-order accurate ensemble transform particle filters. *SIAM Journal on Scientific Computing* **39** A1834–A1850.
- [2] AMEZCUA, J. and VAN LEEUWEN, P. J. (2014). Gaussian anamorphosis in the analysis step of the EnKF: a joint state-variable/observation approach. *Tellus A: Dynamic Meteorology and Oceanography* **66** 23493.
- [3] ANDERES, E. and CORAM, M. (2012). A general spline representation for nonparametric and semiparametric density estimates using diffeomorphisms. *arXiv:1205.5314*.
- [4] ANDERSON, J. L. (2010). A non-Gaussian ensemble filter update for data assimilation. *Monthly Weather Review* **138** 4186–4198.
- [5] ANDERSON, J. L. (2020). A Marginal Adjustment Rank Histogram Filter for Non-Gaussian Ensemble Data Assimilation. *Monthly Weather Review* **148** 3361–3378.
- [6] BAPTISTA, R., ZAHM, O. and MARZOUK, Y. (2020). An adaptive transport framework for joint and conditional density estimation. *arXiv preprint arXiv:2009.10303*.

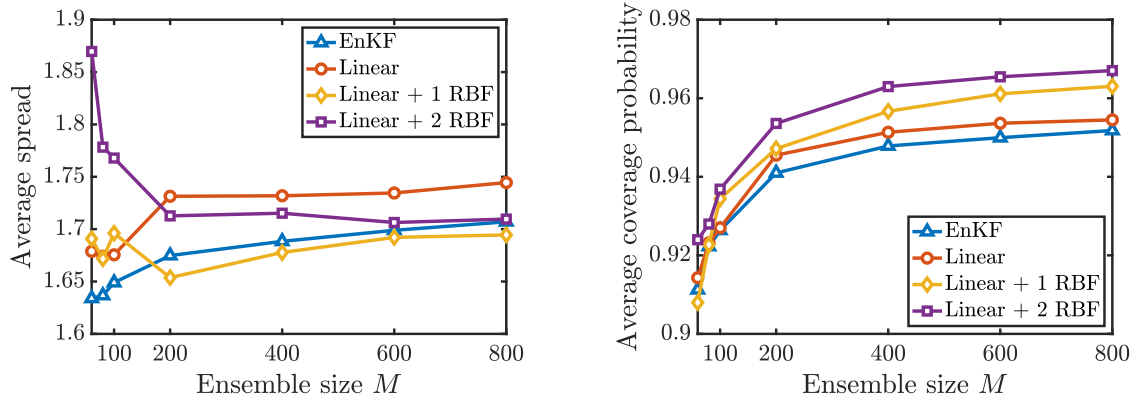


Fig 18: Average ensemble spread (*left*) and average coverage probability of the [2.5%, 97.5%] empirical intervals of each state marginal (*right*) for the Lorenz-96 configuration of Section 4.3, with long inter-observation times, modified to have $d = 20$ square-root observations of the state.

- [7] BENGTSOON, T., SNYDER, C. and NYCHKA, D. (2003). Toward a nonlinear ensemble filter for high-dimensional systems. *Journal of Geophysical Research: Atmospheres* **108**.
- [8] BERTSEKAS, D. P. (1982). Projected Newton methods for optimization problems with simple constraints. *SIAM Journal on control and Optimization* **20** 221–246.
- [9] BICKEL, P. J. and LEVINA, E. (2008). Regularized estimation of large covariance matrices. *The Annals of Statistics* **36** 199–227.
- [10] BIGONI, D., SPANTINI, A. and MARZOUK, Y. (2019). On the computation of monotone transports. *In preparation*.
- [11] BOGACHEV, V. I., KOLESNIKOV, A. V. and MEDVEDEV, K. V. (2005). Triangular transformations of measures. *Sbornik: Mathematics* **196** 309.
- [12] BOX, G. E. and COX, D. R. (1964). An analysis of transformations. *Journal of the Royal Statistical Society. Series B (Methodological)* 211–252.
- [13] BRENNAN, M., BIGONI, D., ZAHM, O., SPANTINI, A. and MARZOUK, Y. (2020). Greedy inference with structure-exploiting lazy maps. In *Advances in Neural Information Processing Systems* 8330–8342.
- [14] BRÖCKER, J. (2012). Evaluating raw ensembles with the continuous ranked probability score. *Quarterly Journal of the Royal Meteorological Society* **138** 1611–1617.
- [15] BURGERS, G., JAN VAN LEEUWEN, P. and EVENSEN, G. (1998). Analysis scheme in the ensemble Kalman filter. *Monthly weather review* **126** 1719–1724.
- [16] CHORIN, A. J. and TU, X. (2009). Implicit sampling for particle filters. *Proceedings of the National Academy of Sciences* **106** 17249–17254.
- [17] CRANMER, K., BREHMER, J. and LOUPPE, G. (2020). The frontier of simulation-based inference. *Proceedings of the National Academy of Sciences* **117** 30055–30062.
- [18] CRISAN, D. and DOUCET, A. (2002). A survey of convergence results on particle filtering methods for practitioners. *IEEE Transactions on Signal Processing* **50** 736–746.
- [19] CUI, T., MARTIN, J., MARZOUK, Y., SOLONEN, A. and SPANTINI, A. (2014). Likelihood-informed dimension reduction for nonlinear inverse problems. *Inverse Problems* **30** 114015.
- [20] DAUM, F. and HUANG, J. (2008). Particle flow for nonlinear filters with log-homotopy. In

- SPIE Defense and Security Symposium* 696918–696918. International Society for Optics and Photonics.
- [21] DEL MORAL, P., KURTZMANN, A. and TUGAUT, J. (2017). On the stability and the uniform propagation of chaos of a class of extended ensemble Kalman–Bucy filters. *SIAM Journal on Control and Optimization* **55** 119–155.
 - [22] DETOMMASO, G., CUI, T., MARZOUK, Y., SPANTINI, A. and SCHEICHL, R. (2018). A Stein variational Newton method. In *Advances in Neural Information Processing Systems* 9169–9179.
 - [23] DOUCET, A. and JOHANSEN, A. M. (2009). A tutorial on particle filtering and smoothing: Fifteen years later. *Handbook of nonlinear filtering* **12** 3.
 - [24] DOUGLAS, R. J. (1999). Applications of the Monge–Ampère equation and Monge transport problem to meteorology and oceanography. In *Monge Ampère Equation: Applications to Geometry and Optimization* **226** 33. American Mathematical Soc.
 - [25] DURBIN, J. and KOOPMAN, S. J. (2012). *Time series analysis by state space methods* **38**. Oxford University Press.
 - [26] EVENSEN, G. (2007). *Data Assimilation*. Springer.
 - [27] FREI, M. and KÜNSCH, H. R. (2013). Bridging the ensemble Kalman and particle filters. *Biometrika* **100** 781–800.
 - [28] GNEITING, T., BALABDAOUI, F. and RAFTERY, A. E. (2007). Probabilistic forecasts, calibration and sharpness. *Journal of the Royal Statistical Society: Series B (Statistical Methodology)* **69** 243–268.
 - [29] GOODFELLOW, I., POUGET-ABADIE, J., MIRZA, M., XU, B., WARDE-FARLEY, D., OZAIR, S., COURVILLE, A. and BENGIO, Y. (2014). Generative adversarial nets. In *Advances in neural information processing systems* 2672–2680.
 - [30] GORDON, N. J., SALMOND, D. J. and SMITH, A. F. (1993). Novel approach to nonlinear/non-Gaussian Bayesian state estimation. In *IEE Proceedings F-radar and signal processing* **140** 107–113. IET.
 - [31] HASTIE, T., TIBSHIRANI, R., FRIEDMAN, J. and FRANKLIN, J. (2005). The elements of statistical learning: data mining, inference and prediction. *The Mathematical Intelligencer* **27** 83–85.
 - [32] HENG, J., DOUCET, A. and POKERN, Y. (2015). Gibbs flow for approximate transport with applications to Bayesian computation. *arXiv:1509.08787*.
 - [33] HOUSSEINEAU, J., JASRA, A. and SINGH, S. S. (2018). Multilevel Monte Carlo for smoothing via transport methods. *SIAM Journal on Scientific Computing* **40** A2315–A2335.
 - [34] HOUTEKAMER, P. L. and MITCHELL, H. L. (2001). A sequential ensemble Kalman filter for atmospheric data assimilation. *Monthly Weather Review* **129** 123–137.
 - [35] JAINI, P., SELBY, K. A. and YU, Y. (2019). Sum-of-Squares Polynomial Flow. In *International Conference on Machine Learning*. arXiv:1905.02325.
 - [36] KAIPIO, J. and SOMERSALO, E. (2007). Statistical inverse problems: discretization, model reduction and inverse crimes. *Journal of computational and applied mathematics* **198** 493–504.
 - [37] KANTOROVICH, L. V. (1965). *The best use of economic resources*. Oxford & London: Pergamon Press.
 - [38] KATZFUSS, M., STROUD, J. R. and WIKLE, C. K. (2020). Ensemble Kalman methods for high-dimensional hierarchical dynamic space-time models. *Journal of the American Statistical Association* **115** 866–885.
 - [39] KIM, S., MA, R., MESA, D. and COLEMAN, T. (2013). Efficient Bayesian Inference Methods via Convex Optimization and Optimal Transport. In *IEEE Symposium on Information Theory* **6**.

- [40] KOLLER, D. and FRIEDMAN, N. (2009). *Probabilistic graphical models: principles and techniques*. MIT press.
- [41] LAURITZEN, S. L. (1996). *Graphical models*. Oxford University Press.
- [42] LAW, K. J. and STUART, A. M. (2012). Evaluating data assimilation algorithms. *Monthly Weather Review* **140** 3757–3782.
- [43] LE PROVOST, M., BAPTISTA, R., MARZOUK, Y. and ELDREDGE, J. (2021). A low-rank nonlinear ensemble filter for vortex models of aerodynamic flows. In *AIAA Scitech 2021 Forum* 1937.
- [44] LEI, J. and BICKEL, P. (2011). A moment matching ensemble filter for nonlinear non-Gaussian data assimilation. *Monthly Weather Review* **139** 3964–3973.
- [45] LINDGREN, F., RUE, H. and LINDSTRÖM, J. (2011). An explicit link between Gaussian fields and Gaussian Markov random fields: the stochastic partial differential equation approach. *Journal of the Royal Statistical Society: Series B* **73** 423–498.
- [46] LIU, Q. and WANG, D. (2016). Stein variational gradient descent: a general purpose Bayesian inference algorithm. In *Advances in Neural Information Processing Systems* 2370–2378.
- [47] LORENZ, E. N. (1963). Deterministic nonperiodic flow. *Journal of the atmospheric sciences* **20** 130–141.
- [48] LORENZ, E. N. (1996). Predictability: A problem partly solved. In *Proc. Seminar on predictability* **1**.
- [49] MAJDA, A. J. and HARLIM, J. (2012). *Filtering complex turbulent systems*. Cambridge University Press.
- [50] MANDEL, J., COBB, L. and BEEZLEY, J. D. (2011). On the convergence of the ensemble Kalman filter. *Applications of Mathematics* **56** 533–541.
- [51] MARIN, J. M., PUDLO, P., ROBERT, C. P. and RYDER, R. J. (2012). Approximate Bayesian computational methods. *Statistics and Computing* **22** 1167–1180.
- [52] MARZOUK, Y., MOSELHY, T., PARNO, M. and SPANTINI, A. (2016). An introduction to sampling via measure transport. In *Handbook of Uncertainty Quantification*.
- [53] METREF, S., COSME, E., SNYDER, C. and BRASSEUR, P. (2014). A non-Gaussian analysis scheme using rank histograms for ensemble data assimilation. *Nonlinear Processes in Geophysics* **21** 869–885.
- [54] MONGE, G. (1781). *Mémoire sur la théorie des déblais et des remblais*. De l’Imprimerie Royale.
- [55] MORZFELD, M., TU, X., ATKINS, E. and CHORIN, A. J. (2012). A random map implementation of implicit filters. *Journal of Computational Physics* **231** 2049–2066.
- [56] MOSELHY, T. and MARZOUK, Y. (2012). Bayesian inference with optimal maps. *Journal of Computational Physics* **231** 7815–7850.
- [57] NINO-RUIZ, E. D., SANDU, A. and DENG, X. (2018). An Ensemble Kalman Filter Implementation Based on Modified Cholesky Decomposition for Inverse Covariance Matrix Estimation. *SIAM Journal on Scientific Computing* **40** A867–A886.
- [58] PARNO, M. and MARZOUK, Y. (2018). Transport map accelerated Markov chain Monte Carlo. *SIAM/ASA Journal on Uncertainty Quantification* **2** 645–682.
- [59] POTERJOY, J. (2016). A localized particle filter for high-dimensional nonlinear systems. *Monthly Weather Review* **144** 59–76.
- [60] PRESS, W. H., TEUKOLSKY, S. A., VETTERLING, W. T. and FLANNERY, B. P. (2007). *Numerical recipes: The art of scientific computing. Third edition*. Cambridge University Press.
- [61] PULIDO, M. and VANLEEUEWEN, P. J. (2018). Kernel embedding of maps for sequential Bayesian inference: The variational mapping particle filter. *arXiv preprint arXiv:1805.11380*.
- [62] RAMSAY, J. O. (1998). Estimating smooth monotone functions. *Journal of the Royal Statistical Society: Series B* 365–375.

- [63] REICH, S. (2013). A nonparametric ensemble transform method for Bayesian inference. *SIAM Journal on Scientific Computing* **35** A2013–A2024.
- [64] REICH, S. and COTTER, C. (2015). *Probabilistic Forecasting and Bayesian Data Assimilation*. Cambridge University Press.
- [65] REZENDE, D. J. and MOHAMED, S. (2015). Variational inference with normalizing flows. *arXiv:1505.05770*.
- [66] ROSENBLATT, M. (1952). Remarks on a multivariate transformation. *The Annals of Mathematical Statistics* 470–472.
- [67] SÆTROM, J. and OMRE, H. (2011). Ensemble Kalman filtering with shrinkage regression techniques. *Computational Geosciences* **15** 271–292.
- [68] SANTAMBROGIO, F. (2015). *Optimal Transport for Applied Mathematicians* **87**. Springer.
- [69] SNYDER, C., BENGTSSON, T., BICKEL, P. and ANDERSON, J. (2008). Obstacles to high-dimensional particle filtering. *Monthly Weather Review* **136** 4629–4640.
- [70] SPANTINI, A. (2017). On the low-dimensional structure of Bayesian inference PhD thesis, Massachusetts Institute of Technology.
- [71] SPANTINI, A., BIGONI, D. and MARZOUK, Y. (2018). Inference via low-dimensional couplings. *The Journal of Machine Learning Research* **19** 2639–2709.
- [72] SPANTINI, A., SOLONEN, A., CUI, T., MARTIN, J., TENORIO, L. and MARZOUK, Y. (2015). Optimal low-rank approximations of Bayesian linear inverse problems. *SIAM Journal on Scientific Computing* **37** A2451–A2487.
- [73] TIPPETT, M. K., ANDERSON, J. L., BISHOP, C. H., HAMILL, T. M. and WHITAKER, J. S. (2003). Ensemble square root filters. *Monthly Weather Review* **131** 1485–1490.
- [74] UENO, G. and TSUCHIYA, T. (2009). Covariance regularization in inverse space. *Quarterly Journal of the Royal Meteorological Society: A journal of the atmospheric sciences, applied meteorology and physical oceanography* **135** 1133–1156.
- [75] VAN LEEUWEN, P. J., KÜNSCH, H. R., NERGER, L., POTTHAST, R. and REICH, S. (2018). Particle filters for applications in geosciences. *arXiv preprint arXiv:1807.10434*.
- [76] VILLANI, C. (2008). *Optimal transport: old and new* **338**. Springer Science & Business Media.
- [77] WACKERNAGEL, H. (1996). Multivariate geostatistics: an introduction with applications. In *International Journal of Rock Mechanics and Mining Sciences and Geomechanics Abstracts* **33** 363A–363A. Springer.
- [78] WRIGHT, S. J. and NOCEDAL, J. (1999). *Numerical Optimization* **2**. Springer New York.
- [79] WU, W. B. and POURAHMADI, M. (2003). Nonparametric estimation of large covariance matrices of longitudinal data. *Biometrika* **90** 831–844.
- [80] YANG, T., MEHTA, P. G. and MEYN, S. P. (2013). Feedback particle filter. *IEEE Transactions on Automatic Control* **58** 2465–2480.